SIMULATIONS OF DROPLET IMPACTS ON HYDROPHOBIC MOVING WALLS

A Thesis

by

Hosein Heidarifatasmi

Submitted to the
Graduate School of Sciences and Engineering
In Partial Fulfillment of the Requirements for
the Degree of

Master of Science

in the
Department of Mechanical Engineering

Özyeğin University
August 2017

SIMULATIONS OF DROPLET IMPACTS ON HYDROPHOBIC MOVING WALLS

Approved by:

Asst. Professor Özgür Ertunç, Advisor
Department of Mechanical Engineering
Özyeğin University

Asst. Professor Altuğ Melik Başol
Department of Mechanical Engineering
Özyeğin University

Asst. Professor Ayşe Gül Güngör
Department of Astronautical Engineering
Istanbul Technical University

Date Approved: 15 August 2017

*To my **mom** and **dad** for their profound support*

ABSTRACT

Numerical simulations of water drop impact onto hydrophobic surfaces (Wax, Teflon) are carried out through usage of Eulerian multiphase model. Volume of fluid (VOF) model is used to capture the deformation of the water drop interface. Importance of contact angle and viscous flow modeling are shown by taking static contact angle (SCA)/dynamic contact angle (DCA) approaches and laminar/turbulent flow regimes respectively. Two and three dimensional simulations are conducted. Validation of the numerical scheme is done successfully by comparing the results of the simulation of impact to static walls with those from the experiments of R. Rioboo, M. Marengo & C. Tropea, Experiments in Fluids, 33, 112(2002). Internal flow of the liquid during the process of impact to static wall is analyzed, particularly for the case of partial rebound. It is observed that the flow structures in the droplet next to the contact line can prevent total rebound. For the moving wall case, partial rebound, deposition and split deposition phenomena are observed as was documented by the experimental study of R. H. Chen, H. W. Wang, Experiments in Fluids, 39, 754(2005). As expected, at high tangential We numbers, the tangential motion of the wall stretches the droplet in the motion direction and causes splitting. In split deposition case, the role of bubble entrainment in rupturing and splitting was mentioned. Energy profiles in time are plotted for each case to provide insight on the dynamics of impact both for moving or stationary walls. Interestingly, viscous dissipation starts to increase slightly before impact and it shows a sudden increase upon impact in the kinematic phase. In general, the kinetic energy drops first due to dissipation and surface enlargement and, in later stages, it increases as a result of surface motion and droplet retraction. Counter intuitively, as the tangential We is increased, the viscous dissipation attains higher

value and shifts the minimum of kinetic energy profile to an earlier dimensionless time but with a higher value. It is found that the dimensionless time where maximum spread of the droplet happens is less influenced by tangential We number.

ÖZETÇE

Hidrofobik yüzeylere damla çarpışının nümerik simülasyonları Euler çok fazlı akış modeliyle gerçekleştirilmiştir. Damlacık yüzeyindeki deformasyonlar için VOF modeli kullanılmıştır. Temas açısının önemi ve viskoz akış modellemeri ayrı ayrı statik temas açısı (SCA) / Dimamik temas açısı (DCA) yaklaşımları ve laminar/türbülanslı akış rejimlerinde incelenmiştir. Simülasyonlar 2 ve 3 boyutlu olmak üzere gerçekleştirilmiş olup kullanılan nümerik yöntemlerin doğruluğu simülasyon sonuçları R. Rioboo, M. Marengo & C. Tropea, Experiments in Fluids, 33, 112(2002) tarafından yapılan statik duvarlara çarpan damlacık deneyi sonuçlarıyla karşılaştırılarak doğrulanmıştır. Statik duvara çarpma sırasında sıvı içerisinde gerçekleşen iç akış özellikle kısmı geri tepme durumları için analiz edilmiştir. Analiz sonucunda, damlacık içerisindeki temas açısında yakın akış yapıları bütün halinde geri tepmeyi engellemektedir. Hareketli duvar durumu içinse; kısmi geri tepme, dağlma, parçalanma gibi oluşumlar R. H. Chen, H.W.Wang, Experiments in Fluids, 39, 754(2005) çalışmasında deneysel olarak gözlenmiştir. Beklenildiği üzere, yüksek yatay We sayılarında duvarın yatay hareketliliği damlacığın hareket doğrultusunda dağılmasına ve parçalanmasına sebebiyet vermektedir. Dağılma durumunda hava kabarcığı varlığının dağılma, sürüklenme ve ayrılma etkilerinden bahsedilmiştir. Her bir durum için zamana bağlı enerji dağılımlarının grafik olarak çıkartılması hem durgun hemde hareketli duvarlarda çarpma dinamiği hakkında görüş sağlamıştır. İlginç biçimde, viskoz dağılma çarpmanın hemen öncesinde çok azda olsa artmaya başlamaktadır ve çarpma anında kinematik safhaya geçince ani bir artış görülmektedir. Genel olarak, kinetik enerji öncelikle dağılma ve yüzey genişlemesinden dolayı azalmakta, sonrasında ise yüzey hareketliliği ve damlacık geri çekilmesinden dolayı artmaktadır. Yatay We sayısı beklenmeyen bir şekilde artmış,

viskoz dağılma daha yüksek değerlere çıkmış ve boyutsuz zaman biriminde minimum kinetik enerji dağılımını daha yüksek değerlerle daha erken safhalara taşımıştır. En çok damlacık dağılmasının yaşandığı boyutsuz zamanda damlacığın yatay We sayısından çok az etkilendiği bulunmuştur.

ACKNOWLEDGEMENTS

I would like to kindly acknowledge my supervisor Asst. Prof. Özgür Ertunç for his limitless help and support not only as an instructor, advisor or supervisor but as a father figure to make a more responsible of me. Of course this accomplishment would not have been possible without his presence. Special thanks to Asst. Prof. Altuğ Melik Başol and Asst. Prof. Ayşe Gül Güngör for their time and consideration as my referees. I would like to gratefully acknowledge TÜBITAK for providing financial support to 114M423 research project. Also, special thanks to Asst. Prof. Dr. Ismail Arı for providing computational resources to carry out numerical simulations.

Finally, I want to heartfully appreciate my parents and specially my little sister for providing their non-stop psychological and emotional support and encouragement throughout all my educational career.

TABLE OF CONTENTS

LIST OF TABLES

LIST OF FIGURES

CHAPTER I

INTRODUCTION

Drop impacts which generally fall into dry solid surface, pre-existed thin liquid film and liquid pool impacts, are of extreme importance and bountiful practical applications in industry such as spray cooling, spray coating, internal combustion engines, prevention of turbine blade erosion and semiconductor and telecommunication industries and also in nature such as absorption of atmospheric gases (CO_2 *or* O_2) on the surface of the seas and oceans, underwater rain noise which is dominated by the bubble entrainment instead of the impact itself and spreading of organism or micro-organism like fungi or small plants like mosses by means of spores.

As mentioned by A. M. Worthington (1852-1916) in his book entitled "A study of splashes" [85], the first careful and deliberate observations of drop impact was done almost twenty years before his book was released by a student at Rugby and reported to the Rugby Natural History Society. Mercury, alcohol, milk and water droplets were tested on smoked glass plate by Worthington and results were depicted in the shape of 197 illustrations from instantaneous photographs which he used electrical sparks for illuminating purposes and was able to achieve exposure times of a few microseconds. Almost 30 years later in October 1936 Harold E. Edgerton released a video containing his famous splashing of the milk drop on a thin film of milk, with his newly stroboscopic and high-speed photography. And later in 1939 Edgerton and James R. Killian published a book entitled "Flash! Seeing the Unseen by Ultra High-speed Photography" full of aforementioned pictures.

Although it might seem the involving phenomena are fairly straightforward and easy to deal with but after years of research, still there is no unique way of representing

different outcomes of drop impact with the existing non-dimensional numbers. This means the underlying physics of the drop impact is still not fully understood and requires more fundamental work in this field.

Upon impact of a drop to a surface, the diversity of parameters affecting the process and the kind of conditions in which the impact is occurring is confounding. The impact might be perpendicular, in an inclined way or even on a moving surface. It might be on the surface of a dry solid object, thin liquid film or a pool of liquid. If the solid dry surface is the case, then the temperature of the surface and drop might be different or the drop might wet a surface partially, completely or construct the lowest surface contact in case of ultrahydrophobic surfaces. The drop might hit a very rough surface or in other extreme it hits a smooth one. On the other hand, if the thin liquid film or liquid pool is the case, then the receiving liquid and drop might be miscible or not. In case of train of drops, generated waves might affect the flow pattern.

In terms of outcomes, considering solid dry surfaces, six disparate outcomes in consequence of drop impact is achieved as demonstrated by Rioboo et al. [59]. The drop might deposit if inertia is weak, undergo either prompt splash (for rough surfaces) or corona splash if inertial forces are prevailing over the surface tension, bounce off the surface in either partial rebound or total rebound mode. Some smaller drops originated from the mother drop might be left behind by the receding lamella which is called receding break up. Or in a special case when the surface temperature is very high (with respect to the drop boiling point), immediately after initial contact, some of the drop fluid will evaporate and acts like an insulating layer which results in preventing the drop from evaporating quickly and helping it to slide on the surface freely which is known as the Leidenfrost effect. But, if we consider the thin liquid film, the consequences are in fact more limited to coalescence or coronet formation, propagation and then breakup. Similarly, in case of a liquid pool a crater may be

formed, ending up with either bubble entrainment or collapsing and creating a central jet which is known as Worthington jet.

However, all the outcomes of the drop impact depends on certain parameters such as drop size, drop velocity, physical properties of drop (such as viscosity and density), surface tension, surface roughness and wettability which is characterized by the static contact angle.

Elasticity in solids helps to not only resist the shear but also recover it at certain extent in time of impact. In contrast, the only force which controls either spreading or contraction of liquid drops is surface tension. As a consequence, in most of the dimensionless numbers that are used in drop impacts, the ratio of different forces is compared with surface tension.

1.1 Non-dimensional Numbers

In general, the main non-dimensional numbers used to characterize drop impact studies are given below

$$\begin{gathered} Re = \frac{\rho DV}{\mu}, We = \frac{\rho DV^2}{\sigma}, Oh = \frac{\mu}{\sqrt{\rho D\sigma}} = \frac{\sqrt{We}}{Re} \\ K = WeOh^{-\frac{2}{5}}, H = \frac{h_0}{D}, Ca = \frac{\mu V}{\sigma} \\ Eo = Bo = \frac{\rho g D^2}{\sigma}, Fr = \frac{V^2}{gD} = \frac{We}{Bo}, R_{nd} = \frac{R_a}{D} \\ We_n = \frac{\rho DV_n^2}{\sigma}, We_t = \frac{\rho DV_t^2}{\sigma} \end{gathered} \tag{1}$$

Where ρ, μ and σ are density, viscosity and surface tension of the liquid drop respectively, D is the drop diameter, R_{nd} is the non-dimensional roughness which is the ratio of the roughness amplitude (R_a) to the drop diameter, and h_0 is the thickness of the thin liquid film. Re, We and Oh are Reynolds, Weber and Ohnesorge number respectively. We_t and We_n are the Weber numbers based on the tangential and normal velocities which are used specifically for drop impacts on inclined or moving surfaces.

K is a combination of non-dimensional numbers which was used by [71, 47, 13] as a splashing/deposition threshold. it will reach to a plateau when the length scale of the roughness amplitude is comparable with the drop diameter as [47] noticed no difference for different non-dimensional roughness values. Also, it increases sharply as the non-dimensional roughness parameter decreases. In other words when the length scale of the roughness amplitude is way smaller than the drop diameter there should be more kinetic energy for the drop to splash [13].

Eo, Bo, Fr and Ca are Eotvos, Bond, Froude and capillary numbers respectively. But not all of them are necessary for analysis. If the impact is driven by gravity, then Eo, Bo or Fr numbers can be used. When it comes to impacts on thin liquid films, then non-dimensional height (H) is going to be used. From the abovementioned set of non-dimensional numbers, one can figure out that there are three major forces namely intertial, viscous and capillary forces. The outcome of a drop impact is determined by the interplay of these forces. Higher inertia and weaker capillary forces can lead to lifting off the outer rim of the spreading lamella hence favour corona splashing mechanism in contrast higher viscous forces would reduce the chance of any breakup mechanism.

Most of the authors tried to characterize their impact data in Re, We, Oh and K non-dimensional numbers but in fact the effect of wettability and surface roughness is not involved in these group of non-dimensional numbers. This way the result of the drop impact usually is either splashing or deposition while there exist four extra outcomes (receding breakup, partial rebound, complete rebound and prompt splash which the first three are connected to wettabililty and the last one is directly connected with surface roughness) missing, referring to the work of Rioboo et al. [59].

1.2 Wettability

How a drop reacts at the moment when it is in contact with a solid surface is defined either by Wenzel [82] or Cassie and Baxter [9]. Homogeneous wetting (Wenzel state) is the state that the drop is completely in contact with the solid surface, filling the grooves on the surface. In contrast inhomogeneous wetting regime (Cassie-Baxter state) occurs when the drop sits on top of tiny air bubbles that filled the roughness irregularities. Wenzel [82] states that

$$cos(\theta^*) = r.cos(\theta) \tag{2}$$

Which θ^*, θ are the Wenzel apparent and Young contact angles respectively, and r is the roughness factor which is defined by the ratio of the real surface area to the projected surface area. As there exist roughness for surfaces, r would be greater than unity. This means roughness can make a hydrophobic surface more hydrophobic and a hydrophilic surface more hydrophilic. However, the Cassie-Baxter equation states

$$cos(\theta^*) = r_f f cos(\theta) + f - 1 \tag{3}$$

which θ^*, θ are the Cassie-Baxter apparent and Young contact angles respectively, f is the fraction of the projected area of the surface which is in contact with the liquid, and r_f is the roughness factor of the wet area. It is clear that if $f \to 0$, apparent contact angle approaches π which makes the surface superhydrophobic. It is worth mentioning that both equations are applicable only when the drop size is large enough compared to the roughness size scale, see [84] and [6]. For more information on equilibrium wetting on rough surfaces see [43].

While drop is stationary there are static, advancing and receding contact angles (theoretical and experimental investigation on how they relate to each other can be found in [74] and [12]) associated with it, however, when the contact line is moving

those values will change. Hoffman et al. [32] showed that for a system of liquid-solid-gas when the interfacial and viscous forces are prevailing, apparent contact angle is changing with Capillary number plus a shift factor which considers the interfacial force between three phases at junction.

The complexity of dealing with the drop impact on dry solid surfaces is not only because of high number of parameters affecting the observed phenomena but also from the interrelation of different parameters to each other as well. To make it clear, decreasing or increasing the surface tension affects wettability characteristics or increasing the roughness will increase the contact angle hysteresis.

Single and train of drops hitting on a thin liquid film were investigated by Stow, C.D., Stainer [72], Cossali et al. [13], Wang and Chen [81], Rioboo et al. [61] and Yarin and Weiss [86] respectively. Experimental velocity criterion for splashing were suggested by Yarin and Weiss [86] and Cossali et al. [13] for train and single drops correspondingly. Also, in a review paper by Yarin [87] it is mentioned that the data obtained for low viscosity liquids from [81] and [61] are in legitimate agreement with the equation suggested by [13]. All those researchers used dimensionless height ($H = h_0/D$) as the ratio of liquid film thickness to the drop diameter in order to classify the impact as thin liquid film when it is less than unity. Generally these type of impacts will end up with deposition which is used by [61] as no rim is visible, spreading which is used by [87] as outer rims are noticeable or splashing. Gregory et al. [24] stated that the number of ejected drops increases as the drop size and velocity of the drop increases or the thickness of the liquid film decreases. Hobbs and Osheroff [30] confirmed the escalation of secondary drops as a result of liquid thickness reduction but further investigated the changes made to crown formation and the Rayleigh jet. Later, Stow, C.D., Stainer [72] mentioned that the number of secondary drops created after the impact is increased by increasing the drop velocity, drop size and surface roughness. Reduction in the number of secondary drops observed by decreasing the

surface tension and increasing the film thickness. More information on thickness and height of the formed crowns, number of jets and secondary droplet sizes can be found in [14].

1.3 Drop Impacts On Moving Surfaces

Drop impacts on moving surfaces were investigated by a few researchers [11, 3, 18, 88]. Partial rebound, deposition and split deposition were the outcomes of water drop impacts on a Teflon surface [11]. From their figures it is seen that the partial rebound happens at low We_t values together with the relatively high We_n numbers. Less energetic impacts would end up with deposition on the surface while split deposition which is disintegration of the water drop into two smaller drops happens at high We_t numbers. Semi-empirical relations were devised to classify the outcomes in We_n and We_t domain. However, deviation from the experimental data in split deposition regime while $We_n < 40$ is quite clear which means the current method is not good at categorizing the physical observations.

Bird et al. [3] examined the splashing regime for impacts with tangential velocity created by either an inclined surface or a moving disk. What they observed is below the splashing threshold, at sufficiently high tangential velocities, the portion of the lamella which is spreading in the opposite direction of the moving surface can experience splashing while the other portion which moves in the same direction experiences only spreading. Similarly, above the splashing threshold, at sufficiently high tangential velocities, one can suppress the splashing in the portion of the lamella which moves in the same direction as the moving surface whereas amplifying the splashing effect on the other side. They came up with a physical model to enhance the efficiency of previous splashing criteria which were the same as the normal impact criteria but modified only by defining the We based on the tangential velocity. Finally they ended up with the following splashing criterion:

$$WeRe^{\frac{1}{2}}(1 - k\frac{V_t}{V_n}Re^{-\frac{1}{2}})^2 = K \tag{4}$$

Where k is a scaling constant of the order one and K is the threshold constant which they mentioned that any parameter that enhances the perturbations in the lamella spreading phase will affect this number. Suggested values of $k = 2.5$ and $K = 5700$ are in good agreement with their experimental data. Care must be taken in analyzing their data because their We and Re numbers are defined with the radius of the drop as the length scale instead of the drop diameter. Note as V_t goes to zero, the equation changes its shape into the previous suggested form.

[88] studied the drop impacts on inclined and moving surfaces. Because of wettability compatibility of the ethanol and the silicon wafer surface they did not observe any rebound outcomes but instead they were able to characterize deposition and splashing phenomena. In their first set of experiments the drop impacts had been conducted on non-moving tilted surfaces to observe the effect of inclination angle on outcomes. The normal component of the We number was used to distinguish different outcomes and yet it was confirmed that $We = 210$ is a good threshold for occurrence of splashing for all different incline angles. Prevention of splashing at both sides due to parallel-to-surface component of the gravity which leads to the so called asymmetric splashing, was called splash-down whilst splash-around referred to splash at both sides. They observed, an increase in inclination angle leads to wider range of asymmetric splashing region which means more inertia is needed to create a two-side splash. In their second set of experiments impacts on horizontal moving surface was investigated. Provoking effect of the moving surface below the splashing threshold and restraining effect of it above the threshold in creating the one-side splashes, were confirmed. Also it was shown qualitatively that at lower We values the range of side-splash is expanded. Using the gravity and moving surface effect in an opposing way where they cancel each others effect was the last part of their experiments which

resulted in a more stretched deposition regime.

Fathi et al. [18] investigated the case of train of drops impacting on a moving surface where the frequency of their piezo element for creating stable jets, was ranging between $9 - 18\ kHz$. The nature of their investigation dictates that not only the kinetic energy of each individual drop is important but rather the rate of energy which is simply the multiplication of the each drop kinetic energy by the frequency of the generated drops, is of desire. In a set of qualitative figures they showed that the increase in frequency will lead to decrease in drop size, increase in drop impingement rate and has almost no effect on drop velocity and flow rate. A new parameter which contained the effects of the impingement rate, volume of the spreading drop and surface velocity, was suggested as the linear deposition rate which was defined as the volume of the deposited fluid to the unit displacement of the moving surface. Intuitively, an increase in surface motion speed will decrease the linear deposition rate but changing the frequency from 12 to 18 kHz had almost no effect on the behavior of the linear deposition rate. They reported generation of a periodic crown-like wave in the advancing liquid layer for high linear deposition rates in contrast to the low values. Also, at high surface velocities and high drop generation frequencies there exist the liquid build up in the progressing layer. Interestingly, the thickness of the spreading liquid layer converged to a constant value for surface velocities higher than a specific threshold for both 12 and 18 kHz frequencies. Anyway, they were unable to find a relation between the number of impinging drops which formed the wave and the surface velocity. Finally they discussed some ambiguities like the increase in the maximum height of the generated wave by increasing the surface speed while the common sense expects reduction of material build-up in the advancing front.

1.4 Theoretical and Numerical Considerations

Removing stress singularity at the contact line and finding a relationship between the dynamic contact angle and the velocity of the contact line are the most critical aspects in dealing with drop impact analyses theoretically and numerically. Theoretical hydrodynamic analysis breaks down in cases of droplet impacts on solid surfaces due to the presence of stress singularity at the three phase boundary. Slippage boundary condition is used in the vicinity (to the slip length extent) of contact line and no-slip boundary condition is used in regions with greater distance than slip length from the three phase boundary, by Cox [15], Foister [19], Hocking and Rivers [31], Shikhmurzaev [67] ,to circumvent this singularity. This type of boundary condition with singular perturbation methods [80] can lead to hydrodynamic solutions to drop impacts, which is discussed in depth in Cox [15]. Another key problem in numerical treatment of droplet impacts is the way that contact angle is modeled. Some studies have used a constant contact angle (equilibrium contact angle) in their numerical scheme [57] while others [41] used two constant values (advancing and receding contact angles) to simulate the phenomena. However, it is observed that receding phase, which starts after the maximum drop spreading, plays an imperative role in impact scenarios and basically determines what type of outcome is going to be expected [60]. As a result, researchers were trying to model the wettability effects in a way that the changes of advancing and receding contact angles reflect themselves as a volumetric force term in momentum equation. A linear relationship between the contact line velocity (local capillary number) and contact angle along with a finite element method developed for free surface flows, is discussed in two complementary papers by Baer et al. [1], Cairncross et al. [8]. Stability of their numerical scheme was an issue as Capillary number increased. Visual discrepancy between experimental tests and predicted results by their method is visible. Also, results of that work were not analyzed thoroughly to extract meaningful physical explanations as it was not in

their scope. Sikalo et al. [68] have used the most recent Kistler model [33] in order to keep track of the changes in advancing and receding contact angles in their two dimensional axisymmetric simulations. From their comparison between experimental and computational results (water drop on Wax surface) one can clearly understand that the behavior of the simulated drop deviates from the real case when it comes to receding phase and secondary drop ejaculation.

Front tracking, level-set, VOF and lattice-Boltzmann methods are available numerical algorithms to deal with multiphase flows. Level-set methods are powerful tools for analyzing and tracking the interface for evolving topologies in time based on an Eulerian approach [66]. Numerical studies of drop impacts have been done by several researchers [2, 42, 48, 78]. Lunkad et al. [42] simulated the drop impacts on horizontal and inclined solid surfaces with VOF method for different wettability conditions. Their results were predicting good for non-wettable surfaces while they could not capture physical phenomena in wettable surfaces. Gunstensen et al. [26] proposed a lattice-Boltzmann method for simulations of two immiscible fluids and through the numerical simulations they could estimate the surface tension coefficient for fluids in motion and stationary cases. Later, Grunau et al. [25] extended the proposed method to consider the density and viscosity variations. A thorough explanation of the lattice-Boltzmann method and its shortcomings and benefits can be found in [49]. Bararnia et al. [2] were using lattice-Boltzmann method to perform the simulations of falling drops. Hence considering the effect of gravitational and surface forces using Eotvos number. They showed the rate of deformation has direct proportionality to Eotvos number. In other words, the more the Eotvos number, the more is the deformation. Tryggvason et al. [78] used a front tracking method to capture any change in the interface by taking the whole domain as one fluid with different physical properties and added the interfacial interactions between two phases with

source terms in their equations. Effect of Re number on maximum spreading diameter of the drop and We number on the time scales of reaching to the maximum drop spreading and equilibrium conditions were investigated by Muradoglu and Tasoglu [48]. It was stated that there is a threshold for Re number in which passing that criterion would result in no serious effect on maximum drop spreading and also as We number increases the mentioned time scales increase as well. Their model was based on the front tracking method developed by [79] tested with analytical solutions at two extremes ($Eo >> 1$ and $Eo << 1$) and finally was showing a good agreement with the experimental data of [69].

Due to complications of the method used in [79] while adding/subtracting points to/from the moving grid, a level-set method was introduced by [50] which is taking care of merging and breaking the interface and also it circles the problem of adding/subtracting points mentioned before. Applications of implementing level-set methods can be found in [73].

Fukai et al. [22] proposed a theoretical model to account for inertia, gravitational effect, surface tension and wetting characteristics of the surface in drop impacts on a horizontal surface. However, they used advancing and receding contact angles of a drop sliding slowly over an inclined surface as the advancing and receding contact angles in their model which we know that those values will change whenever the contact line velocity is changing. As a result, they found that the wettability of the surface is going to affect the spreading process significantly. In a study done by Lunkad et al. [42] the drop impact on horizontal and inclined surfaces was simulated using both SCA and DCA approaches. It was found that the SCA model is well predicting the spreading behavior for non-wettable surfaces but it was unable to give good results for wettable surfaces due to one order of magnitude difference between DCA and SCA for wettable surfaces at early stages of impact. Due to the same issue they were unable to capture splashing, rebounding and deformation regimes with

their computational model. Also, Over-predicting of the spreading factor was another consequence of the same issue. Effect of surface tension and contact angle in dynamics of the impacting drop was studied in [51] by means of adding different concentrations of a surfactant. It turned out adding the surfactant has no significant effect on the initial spreading of the drop however, it changes the receding phase in a noticeable manner. Moreover, reduction in equilibrium contact angle was seen while no notable change was happening in advancing contact angle as a consequence of adding the surfactant. Simulations of moving contact lines with the usage of VOF method was done by [57] Their method was corrected to enforce the mass conservation and also the gradients of volume fraction was differently treated next to the boundaries.

The effect of impact velocity of the drop on behavior of air entrapment is imperative. For low velocities of impacting drop in case of drop impacts on liquid pools the air film can be stretched in such a way that the drop even does not touch the liquid pool hence bouncing off the surface of the liquid pool. In contrast, for high velocities, the air film is going to rupture and it is shown that the higher the impact velocity the thicker would be the thickness of air film at the instant of rupturing. Because of the excessive velocity the air does not have time to be squeezed between the drop and surface of the liquid pool consequently ruptures at larger thicknesses [77]. The thickness of air film is in the range of 2-5 μm for drop impacts on solid surfaces while it is 1-2.5 μm for drop impacts on liquid pools [76]. As the drop is traveling towards the solid surface, the air between the solid surface and drop is going to be pressurized and since the only side which is deformable is the drop side, it will flatten the bottom side of the drop causing the contact in a circular shape instead of a point [44]. This will cause bubble entrapment right at the center of the drop at early stages of impact.

1.5 Objective

The ultimate objective of the present work is to simulate the impact outcomes of water droplet impacts on hydrophobic surfaces whether they are stationary or moving linearly with a constant speed. Dynamics of such impacts is of interest which is going to be obtained by spreading dynamics, flow analysis and energy analysis of different scenarios of impacts.

1.6 Hypothesis

As mentioned in the context of this chapter, knowing how different forms of energy dynamically behave in different impact scenarios (stationary and moving), would give us insights on the nature of these impacts. Questions on what would be the effect of bubble entrapment during an impact cycle, what would be the key differences between impacts on stationary surfaces compared to moving ones or how flow structures can prevent or trigger droplet rebound and more interesting questions are going to be answered at least partially in the present work.

1.7 Methodology

To achieve such a goal we are going to take advantage of numerical tools to discover the truth behind those questions. Among the numerical methods to treat multiphase flows we have chosen volume of fluid (VOF) method to simulate the phenomena of droplet impacts onto solid surfaces. This thesis is going to address the effect of surface motion on dynamics of drop impacts on hydrophobic surfaces particularly by exploiting energy and flow analyses of such impact scenarios.

1.8 Thesis Structure

In that sense, Chapter 2 is going to present basics of our numerical modeling particularly volume of fluid (VOF) method and Kistler contact angle modeling. Chapter 3 deals with validation of our numerical tool plus some information on impacts on

non-moving walls. While Chapter 4 takes care of impacts on moving surfaces in different possible regimes for a hydrophobic surface. Sections 3.3 and 4.3 provide the results and show this study tries to gain insight in dynamics of drop impacts on stationary and moving surfaces based on the energy distribution and competition of present forces. It is going to be shown that even on the cases where the We number is high (which means inertial forces are dominating), the calculation of contact angle is still a crucial task. At the final stages of spreading and the whole receding phase (if exists any), it is this capillary forces which has to be modeled carefully in order to obtain similar physical behavior of drop impacts. Also, it is interesting to track the dynamics of the contact line (how contact angle changes with time) for a constant normal We number but with different surface velocities. Effect of bubble entrapment (motion, coalescence and escape of the bubbles) on dynamics of droplet (rupture at the surface of the spreading drop and change in contact angle due to the motion of the bubbles close to the contact line) impacts is going to be addressed in the current work as well. And, final remarks are going to be made in chapter 5 as closing words at the end of this thesis.

CHAPTER II

NUMERICAL MODELING

2.1 Volume of Fluid (VOF) Method

Numerical basis of VOF method is originated from a numerical solution algorithm (known as SOLA) for un-steady flows (see [29]) in which it is based on a much more complicated and hard to implement marker and cell method (MAC). It can be used for both confined flows and free surface flows. However, the first version of SOLA-VOF was published in the work of [28]. Since for the problems where free boundaries experience large deformations, usage of Lagrangian methods would face not much of an achievement hence, Eulerian formulations are used instead. After velocities are computed, one needs to calculate the fluid flow through the mesh in an Eulerian approach. And this is going to be done by calculating some convective fluxes in which an averaging of the flow properties of all fluid elements in a given cell is unavoidable. It is this process which makes a drawback of Eulerian methods since it creates a smearing of discontinuous surface (free surfaces).

One method to treat free surface flows is through usage of the so-called height functions. In that method the distance of the interface with respect to a reference line (h) is going to be stored as a function of position. The advantage of this method is that it is computationally efficient because one needs to only store a one-dimensional array of the height values to represent the free surface. However, one serious drawback of this method is that it does not work when $\frac{dh}{dx}$ exceeds the cell aspect ratio ($\frac{\delta y}{\delta x}$) or when you have multiple values of y for a single value of x such as bubbles or droplets. This means it certainly cannot be used for treating drop impact scenarios. To circumvent this problem line segments method is established which uses more

storage capacity but it can deal with multi-valued surfaces. This method uses a series of small line segments to represent the free surface and the evolution of the interface is going to be done by addition/deletion of new line segments. The pitfall of this method is that when we have interface intersections (such as coalescence of droplets), segment chains has to be rearranged. And finally, to tackle this issue the method of marker particles were proposed in which indirectly represents the interface by the concept of marker particles. Marker particles are going to be distributed inside the fluid and moving with the velocity of the fluid itself while interfaces are going to be represented in the regions among with and without marker particles. This clearly shows how this method can become computationally intense. Volume of fluid method was born at this time trying to solve the issue with its proper algorithm.

Volume of fluid uses a function (volume fraction, α) whose value is unity when the cell is occupied by fluid and zero otherwise. And, any cell which contains a value between zero and one is going to be interpreted as a cell which has interface in it. Normal direction to the interface can be found where the value of volume fraction changes with highest slope. This means having normal vector to the free surface and the value of volume fraction in a cell, a line could represent the interface at that cell. However, this is not enough because one needs to track the changes of the interface in time with an advection equation.

$$\frac{\partial \alpha}{\partial t} + u\frac{\partial \alpha}{\partial x} + v\frac{\partial \alpha}{\partial y} = 0 \tag{5}$$

Where u and v are fluid velocities in x and y directions respectively. Note that SOLA-VOF also uses pressure and velocity as its primary dependent variables and the values of the pressures are determined only at the center of the surface containing cell. Equations 6 and 7 are showing the divergence free condition and Navier-Stokes equations of flow motion, respectively.

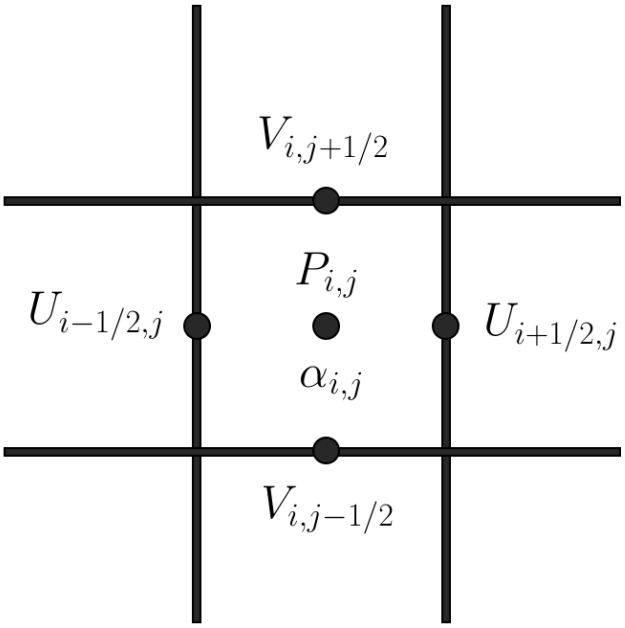

Figure 1: Representation of dependent variables in a sample computational cell.

$$\frac{\partial u}{\partial x} + \frac{\partial v}{\partial y} + \frac{\partial \xi u}{\partial x} = 0 \tag{6}$$

$$\begin{aligned} \frac{\partial u}{\partial t} + u\frac{\partial u}{\partial x} + v\frac{\partial u}{\partial y} &= -\frac{\partial p}{\partial x} + g_x + \nu\Big[\frac{\partial^2 u}{\partial x^2} + \frac{\partial^2 u}{\partial y^2} + \xi\left(\frac{1}{x}\frac{\partial u}{\partial x} - \frac{u}{x^2}\right)\Big] \\ \frac{\partial v}{\partial t} + u\frac{\partial v}{\partial x} + v\frac{\partial v}{\partial y} &= -\frac{\partial p}{\partial y} + g_y + \nu\Big[\frac{\partial^2 v}{\partial x^2} + \frac{\partial^2 v}{\partial y^2} + \frac{\xi}{x}\frac{\partial v}{\partial x}\Big] \end{aligned} \tag{7}$$

Where g_x, g_y, ν and p are gravitational acceleration in x and y direction, kinematic viscosity and pressure, respectively. Also ξ is a constant which has two possible values of zero and unity. If it is zero it represents the equations in Cartesian coordinate system and when it is unity it represents the equations in cylindrical coordinate system. Figure 1 shows the representation of dependent variables in a sample computational cell.

In its original form, one can use finite difference method to discretize Eqs. 6 and 7 which is shown below.

$$\frac{1}{\delta x}\left(u_{i,j}^{n+1}-u_{i-1,j}^{n+1}\right)+\frac{1}{\delta y}\left(v_{i,j}^{n+1}-v_{i,j-1}^{n+1}\right)+\frac{\xi}{2\delta x(i-1.5)}\left(u_{i,j}^{n+1}-u_{i-1,j}^{n+1}\right)=0$$

$$\begin{aligned} u_{i,j}^{n+1} &= u_{i,j}^{n}+\delta t\Big[\frac{1}{\delta x}\left(p_{i,j}^{n}-p_{i+1,j}^{n}\right)+g_x-FUX-FUY-FUC+VISX\Big] \\ v_{i,j}^{n+1} &= v_{i,j}^{n}+\delta t\Big[\frac{1}{\delta y}\left(p_{i,j}^{n}-p_{i,j+1}^{n}\right)+g_y-FVX-FVY-FVC+VISY\Big] \end{aligned} \tag{8}$$

Note that FUX, FUY, FUC, FVX, FVY and FVC are convective fluxes while VISX and VISY are the viscous fluxes which are going to be defined in the following set of equations.

$$\begin{aligned} FUX=\frac{1}{4\delta x}\Big[&\left(u_{i,j}+u_{i+1,j}\right)^2+\beta\mid u_{i,j}+u_{i+1,j}\mid\left(u_{i,j}-u_{i+1,j}\right)\\ &-\left(u_{i-1,j}+u_{i,j}\right)^2-\beta\mid u_{i-1,j}+u_{i,j}\mid\left(u_{i-1,j}-u_{i,j}\right)\Big] \end{aligned} \tag{9}$$

$$\begin{aligned} FUY=\frac{1}{4\delta y}\Big[&\left(v_{i,j}+v_{i+1,j}\right)\left(u_{i,j}+u_{i,j+1}\right)+\beta\mid v_{i,j}+v_{i+1,j}\mid\left(u_{i,j}-u_{i,j+1}\right)\\ &-\left(v_{i,j-1}+v_{i+1,j-1}\right)\left(u_{i,j-1}+u_{i,j}\right)-\beta\mid v_{i,j-1}+v_{i+1,j-1}\mid\left(u_{i,j-1}-u_{i,j}\right)\Big] \end{aligned} \tag{10}$$

$$\begin{aligned} FUC=\frac{\xi}{8\delta x(i-1)}\Big[&\left(u_{i,j}+u_{i+1,j}\right)^2+\left(u_{i-1,j}+u_{i,j}\right)^2+\beta\mid u_{i,j}+u_{i+1,j}\mid\left(u_{i,j}-u_{i+1,j}\right)\\ &+\beta\mid u_{i-1,j}+u_{i,j}\mid\left(u_{i-1,j}-u_{i,j}\right)\Big] \end{aligned} \tag{11}$$

$$\begin{aligned} FVX=\frac{1}{4\delta x}\Big[&\left(u_{i,j}+u_{i,j+1}\right)\left(v_{i,j}+v_{i+1,j}\right)+\beta\mid u_{i,j}+u_{i,j+1}\mid\left(v_{i,j}-v_{i+1,j}\right)\\ &-\left(u_{i-1,j}+u_{i-1,j+1}\right)\left(v_{i-1,j}+v_{i,j}\right)-\beta\mid u_{i-1,j}+u_{i-1,j+1}\mid\left(v_{i-1,j}-v_{i,j}\right)\Big] \end{aligned} \tag{12}$$

$$\begin{aligned} FVY=\frac{1}{4\delta y}\Big[&\left(v_{i,j}+v_{i,j+1}\right)^2+\beta\mid v_{i,j}+u_{i,j+1}\mid\left(v_{i,j}-v_{i,j+1}\right)-\left(v_{i,j-1}+v_{i,j}\right)^2\\ &-\beta\mid v_{i,j-1}+v_{i,j}\mid\left(v_{i,j-1}-v_{i,j}\right)\Big] \end{aligned} \tag{13}$$

$$\begin{aligned} FVC=\frac{\xi}{8\delta x(i-1.5)}\Big[&\left(u_{i,j}+u_{i,j+1}\right)\left(v_{i,j}+v_{i+1,j}\right)+\left(u_{i-1,j}+u_{i-1,j+1}\right)\left(v_{i-1,j}+v_{i,j}\right)+\beta\mid u_{i,j}\\ &+u_{i,j+1}\mid\left(v_{i,j}-v_{i+1,j}\right)+\beta\mid u_{i-1,j}+u_{i-1,j+1}\mid\left(v_{i-1,j}-v_{i,j}\right)\Big] \end{aligned} \tag{14}$$

$$VISX = \nu\Big[\frac{1}{(\delta x)^2}\left(u_{i+1,j} - 2u_{i,j} + u_{i-1,j}\right) + \frac{1}{(\delta y)^2}\left(u_{i,j+1} - 2u_{i,j} + u_{i,j-1}\right) + \frac{\xi}{2(\delta x)^2(i-1)}\left(u_{i+1,j} - u_{i-1,j}\right) - \frac{\xi u_{i,j}}{(\delta x)^2(i-1)^2}\Big] \tag{15}$$

$$VISY = \nu\Big[\frac{1}{(\delta x)^2}\left(v_{i+1,j} - 2v_{i,j} + v_{i-1,j}\right) + \frac{1}{(\delta y)^2}\left(v_{i,j+1} - 2v_{i,j} + v_{i,j-1}\right) + \frac{\xi}{2(\delta x)^2(i-1.5)}\left(v_{i+1,j} - v_{i-1,j}\right) - \frac{\xi u_{i,j}}{(\delta x)^2(i-1)^2}\Big] \tag{16}$$

Where β is the so-called coefficient of donor cell differencing in which when it is equal to zero, equations are going to represent its predecessor marker and cell (MAC) method. Solution procedure breaks down into three main steps. In the first step by applying explicit approximations to Navier-Stokes equations, one needs to compute the first guess for new time level velocities. In the second step to satisfy conservation of mass equation, one needs to adjust the pressure values to have zero divergence and consequently changes in velocity (by adjusting pressure) also need to be added to values obtained in first step. In third and last step α needs to be updated to give the new interface. The sequence would be repeated to march in time. For more information on implementation of this method and some applied examples the reader is encouraged to take a look at [28, 29]. Note that these are the basics of VOF method but the way it is implemented in Star-CCM+ is completely different. Details of the solution algorithm is not available however, the general strategy is discussed in the rest of following section.

Immiscible fluids in a control volume share velocity, pressure and temperature fields as the VOF method in Star-CCM+ is formulated. As a result the same mass, momentum and energy conservation equations that are solved for single phase flow is going to be solved for multiphase flows but the physical properties in the solution domain is varying based on the volume fraction of the constituent phases. Calculation of the physical properties based on the volume fractions of the phases are as follows:

$$\rho = \sum_i \rho_i \alpha_i \tag{17}$$

$$\mu = \sum_i \mu_i \alpha_i \tag{18}$$

where $\alpha_i = \frac{V_i}{V}$, ρ_i and μ_i are the volume fraction, density and dynamic viscosity of the i^{th} phase. Formulation of Conservation of mass and momentum in their integral form is as follows:

$$\frac{\partial}{\partial t}\int_V (\rho\chi)\, dV + \int_A \rho(\mathbf{V} - \mathbf{V}_g)\, dA = \int_V (s_u)\, dV \tag{19}$$

$$\begin{aligned}\frac{\partial}{\partial t}\int_V (\rho\chi\mathbf{V})\, dV + \int_A \rho\mathbf{V}\otimes(\mathbf{V} - \mathbf{V}_g)\, dA + \int_A PI\cdot\, dA = \\ + \int_A T\cdot\, dA + \int_V (f_r + f_g + f_p + f_u + f_\omega + f_L)\, dV\end{aligned} \tag{20}$$

Where $\chi, \mathbf{V}, \mathbf{V}_g, P, I$ and T are the fraction of volume not occupied by porous media, velocity, grid velocity, pressure, identity matrix and viscous stress tensor. Also $f_r, f_g, f_p, f_u, f_\omega$ and f_L represent body force terms related to rotation, buoyancy, porous media, user-defined body forces, vorticity confinement specific force and electromagnetic fields respectively. Usually an advection equation is solved for volume fraction to capture the changes at interface, however, in STAR-CCM+ the integral form of this equation is as follows:

$$\frac{d}{dt}\int_V \alpha_i\, dV + \int_A \alpha_i(\mathbf{V} - \mathbf{V}_g)\, dA = \int_V \left(s_{\alpha_i} - \frac{\alpha_i}{\rho_i}\frac{D\rho_i}{Dt}\right)\, dV \tag{21}$$

In which $\alpha_i, \mathbf{V}, \mathbf{V}_g$ and s_{α_i} are the volume fraction of phase i, velocity, grid velocity and sink or source of the i^{th} phase. The term $\frac{D\rho_i}{Dt}$ is the material derivative of the density of the phase i which contains the temporal and directional derivatives.

Surface tension force is a tensile force tangential to the interface between present phases. In Star-CCM+, it is modeled as a volumetric force using the continuum

surface force (CSF) approach proposed by Brackbill et al. [5]. The magnitude of this force depends on the nature of the immiscible fluids and temperature. The equations regarding to formulation of the surface tension force are as follows:

$$f_\sigma = f_{\sigma,n} + f_{\sigma,t} \; where \; f_{\sigma,n} = \sigma\kappa\mathbf{n}, \; f_{\sigma,t} = \frac{\partial\sigma}{\partial t}t \tag{22}$$

Where σ is the surface tension coefficient. f_σ is the surface tension force in which subscripts of n and t denote the normal and tangential components of this force respectively. $\mathbf{n}$ is the unit vector normal to the interface between phases and directing from liquid to gas phase. t is the unit vector in the tangential direction to the interface and κ is the mean curvature of the interface. CSF model uses the smooth field of the phase volume fraction α_i to calculate the normal vector to the interface. Calculation of the normal vector to the interface and interface curvature is possible through following equations.

$$\mathbf{n} = \nabla\alpha_i \tag{23}$$

$$\kappa = -\nabla \cdot \frac{\nabla\alpha_i}{|\nabla\alpha_i|} \tag{24}$$

The common quantity of many different dynamic contact angle (DCA) correlations is the triplet line velocity which is the line where the solid phase and both fluid phases come into mutual contact. Star-CCM+ implements the Kistler correlation ([33]), which is an empirical DCA correlation based on the capillary number and usage of the Hoffman function. The definition of the Capillary number is given below:

$$Ca = \frac{V\mu}{\sigma} \tag{25}$$

Where V, σ and μ are the triplet line velocity, surface tension force and dynamic viscosity of the primary phase which is water in our simulations. Triplet line velocity

is calculated based on the relative velocity of the fluid and the wall as it is stated below:

$$V = - < V, \hat{n}_t > \tag{26}$$

Where V is the relative velocity of the fluid and the corresponding wall at the triplet line and $\hat{n}_t$ is the normalized wall tangent pointing in the same direction as the volume fraction gradient of the primary phase ($\nabla \alpha_i$).

2.2 Contact Angle Modeling

Definition of the Kistler contact angle is given as follows:

$$\theta_k = f_{Hoff}\left(Ca + f_{Hoff}^{-1}\left(\theta_s\right)\right) \tag{27}$$

$$f_{Hoff}\left(x\right) = \cos^{-1}\left(1 - 2\tanh\left(5.16\left(\frac{x}{1 + 1.31x^{0.99}}\right)^{0.706}\right)\right) \tag{28}$$

Where $\theta_k, \theta_s, f_{Hoff}$ and f_{Hoff}^{-1} are the Kistler contact angle, static contact angle (SCA), Hoffman function and the inverse of the Hoffman function. In order to get a closed form for the inverse of the Hoffman function the software uses x in the denominator instead of $x^{0.99}$. This, is eligible for the contact angle values in the range of 0 to 176 degrees. SCA is going to be substituted based on the sign of the capillary number and its value is either the advancing or receding contact angle. To enhance the stability of the method that is implemented in Star-CCM+, a range for the equilibrium Capillary number can be defined. Within the specified range $-Ca_{eq} < Ca < Ca_{eq}$, the resulting dynamic contact angle is blended with the equilibrium contact angle (θ_e) which is a user-specified value.

$$\theta_d = f\theta_e + (1 - f)\,\theta_k \tag{29}$$

The factor f is going to be determined by the following equation:

$$f = 0.5 + 0.5\cos\left(\frac{Ca}{Ca_{eq}}\pi\right) \tag{30}$$

In order to show the significance of using Kistler model in changing the contact angle values for advancing and receding contact angles one can look at Fig. 2. As it is shown, static advancing contact angle starts from 141 degrees and reaches to 150 when the capillary number reaches to its maximum. Also, static receding contact angle is changing from 81 degrees at zero capillary number and reaches to almost 30 degrees when the capillary number reaches to its minimum while static contact angle will only consider the value of 103 degrees which is the equilibrium contact angle of the water drop on Teflon surface.

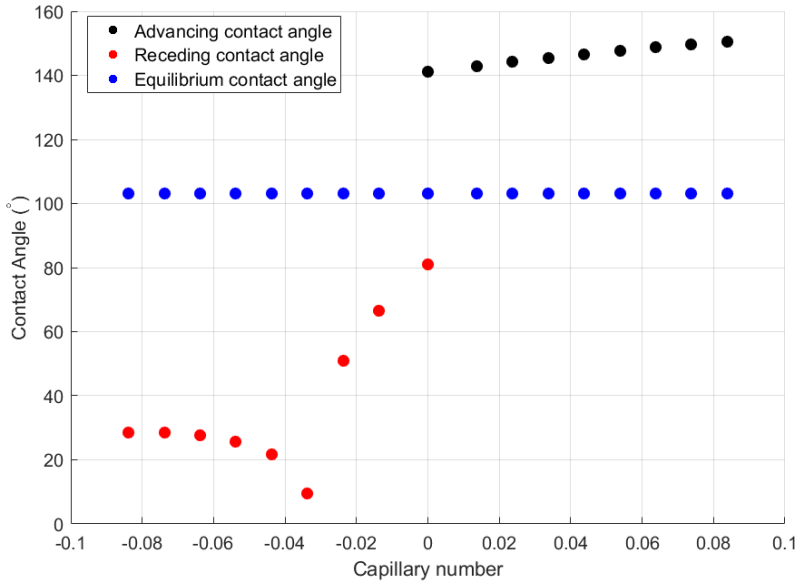

Figure 2: Extent of variation in contact angle through usage of Kistler model. Receding and advancing contact angles of water droplet on Teflon surface are taken from [63]. Capillary values are calculated based on the velocity range from our simulations on moving walls.

CHAPTER III

IMPACTS ON STATIONARY SURFACES

3.1 Problem Statement

Numerical simulations of the drop impact on a surface has been done by a commercial CFD package called StarCCM+. Since $3D$ simulations are requiring more computational resources in the first stages $2D$ simulations have been carried out to verify the physical phenomena caused by drop impacts. And then later, the same validation case is going to be tested with the current numerical scheme but this time considering it in $3D$. The nature of the problem dictates us to use an implicit unsteady scheme as it is a time dependent phenomena. Since the drop is moving inside a medium filled with air the use of Eulerian multiphase model is necessary. Among the available methods for multiphase simulations the VOF model is suitable for our needs. There are number of reasons for this selection which we can summarize them in its simplicity where immiscible phases share velocity, pressure and temperature fields, same set of transport equations for a single phase are solved, physical properties are calculated based on volume fractions and finally surface tension is modeled like a volumetric force, a commonly used approach in VOF ever since developed in 1992 [5]. The effect of surface tension is considered through activating the multiphase interaction feature. In order to start the main simulations regarding the subject of the current thesis, we need to test our numerical tool to make sure that whether we are capable to perform those simulations (particularly on moving and vibrating walls) with a certain degree of confidence or not. To serve that purpose, we need to validate our numerical scheme with existing experimental drop impact scenarios.

Note that in this chapter, results of both $2D$ and $3D$ simulations are provided for

the validated case. In the next section, numerical setup of the problem is going to be constructed. Geometry, boundary conditions and mesh properties of each simulation case is tabulated in the same section. Results of such simulations are going to be shown in section 3.3. And finally, in the last section a brief discussion is going to be made on the obtained results.

3.2 Numerical Setup

Two dimensional ($2D$) axisymmetric and three dimensional ($3D$) simulations of drop impact on non-moving walls were done for validation of the numerical approach. Then, $3D$ models were extended to moving surfaces and the simulations were run for droplet impacts on moving walls. Star-CCM+ 10.06.010 which is a commercial CFD package software was used to perform the mentioned simulations. Eulerian multiphase model was used to define water and air phases and VOF method was used in order to capture the changes at the interface between the two phases.

A field function was written to use bigger time steps whenever it is possible under the condition of keeping the Courant number in the simulations in the range of $0.89-0.99$. Therefore, a range for the maximum and minimum time steps were defined so that the time steps would vary in that range.

3.2.1 Computational Domain

In $2D$ axisymmetric simulations the geometry is a simple rectangular one (see Fig. 3) while in $3D$ computational domain that we used was a rectangular cuboid (see Fig. (4)). Boundary conditions of both $2D$ and $3D$ simulations are given in the same figures. The size of the domain for $2D$ cases was $6.875 \times 8.25\, mm^2$ and for $3D$ one was $6.875 \times 10.3125 \times 9.25\, mm^3$. Dimensions of the domain were determined by the size of the droplet in order to make parametric study for other impact cases easier as we were going to extend these to moving walls.

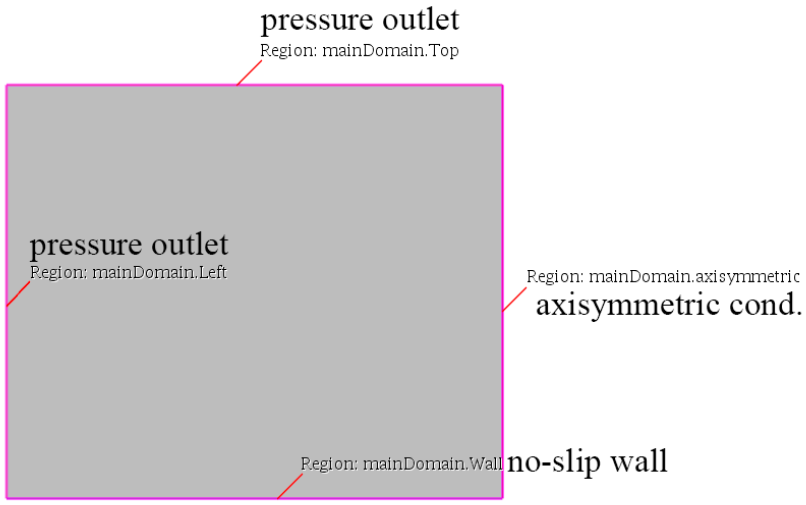

Figure 3: Geometry and boundary conditions of $2D$ axisymmetric simulations for the validated case.

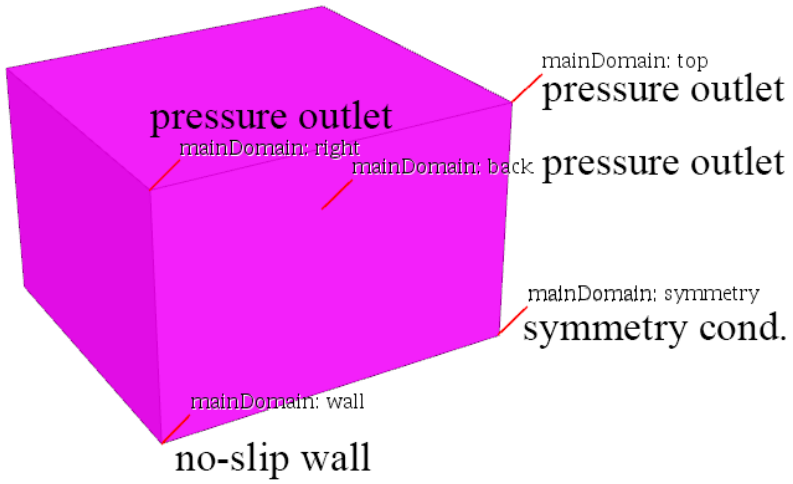

Figure 4: Geometry and boundary conditions of $3D$ simulation for the validated case.

3.2.2 Boundary Conditions

Boundary conditions for both $2D$ and $3D$ cases were shown in previous figures when we presented the characteristics of computational domain for each case. In all outer surfaces of the cuboid, the pressure outlet boundary condition was selected except the one at the bottom on which the wall condition was implemented and the one at the front in which the symmetry condition was applied. In the same manner in all lateral sides of the $2D$ domain pressure outlet boundary condition was selected except for the one at the bottom on which the wall condition was used and the one at the right side in which the axisymettric axis condition was implemented. The value of $0\,Pa$ was entered for the pressure outlet condition with respect to the ambient atmospheric pressure. For the wall, no-slip boundary condition was picked and depending on the DCA or SCA the advancing and receding contact angles or static contact angle was selected, respectively. For SCA condition we were using the value of 100° for equilibrium contact angle and in case of DCA condition, Kistler model was used with 95°, 105° and 100° as receding, advancing and equilibrium contact angles. These values for the case of water droplet on Wax surface were taken from Rioboo et al. [60]. Information on Kistler model and its impact on calculation process can be found in section 3.2.

3.2.3 Mesh Properties

In $2D$ simulations both polyhedral (unstructured) and rectangular (structured) mesh was used as it is shown in Fig. 5. However, care must be taken in using structured mesh for $3D$ simulations since we have observed some kind of directional behaviour in the deformation of the droplet which basically was physically impossible. Although it was giving wrong results in three dimensional cases but it was working perfectly fine in two dimensional cases. As a result only polyhedral mesh was used to mesh the computational domain in $3D$ simulation. And, depending on the size of the

Table 1: Summary of mesh properties for both $2D$ and $3D$ simulations of the validated case.

Type	Domain size [1]	No. of Cells
$2D - structured\,mesh$	2×6	≈ 56000
$2D - unstructured\,mesh$	2×6	≈ 51000
$3D - unstructured\,mesh$	$10 \times 7 \times 9$	≈ 3 million

domains, the number of cells were different. However, the resolution more or less was kept constant for the cases that we have done both $2D$ and $3D$ trials in order to be consistent with the effects of meshing on the solution. Trajectory of the droplet while it is moving towards the surface and also a specific thickness from the wall were resolved more by using custom control mesh size capability in Star-CCM+. The closest distance from the wall for deposition and split deposition cases that we could resolve was 5 μm while this value decreased to 1 μm for the case of partial rebound in chapter 3. Near the wall 5 prism layers were used with aspect ratio of the cells close to 0.6. In the same manner the mesh was created for the $3D$ case and both top and front view of the implemented mesh is shown in Fig. 6. It is worth noting that here the aspect ratio in our prism layers was reduced to 0.3 but it was persuasive enough to fulfill the criteria for validation. Basically, the consequence is less amount of cells and fast computation however it comes with the price of inaccuracy in your final results which in our case the mentioned value was good enough to maintain our criteria for validation.

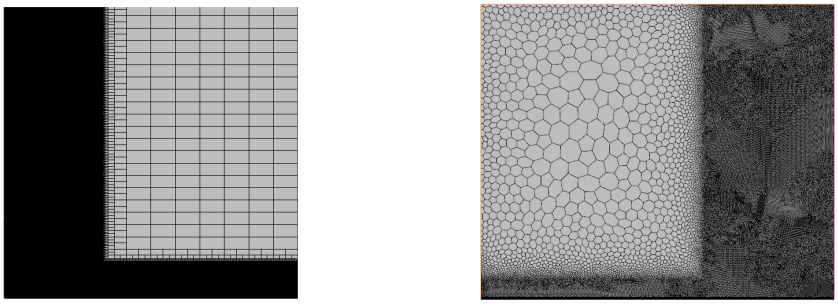

Structured Mesh
(Rectangular cells)

Unstructured Mesh
(Polyhedral cells)

Figure 5: Mesh representation of $2D$ axisymmetric simulations for the validated case.

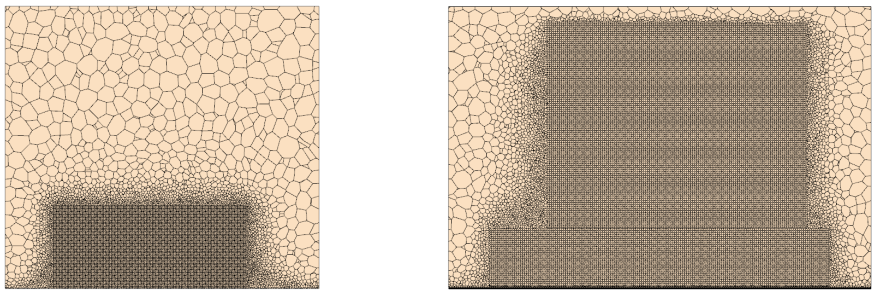

Top view

Front view

Figure 6: Mesh representation of $3D$ simulation for the validated case.

3.3 Results and Discussion

Validation of the numerical scheme was done by simulating the normal drop impacts on a stationary hydrophobic surface which was documented in detail by Rioboo et al. [60]. For the validation, the evolution of the spread factor which is the ratio of the instantaneous spreading diameter (d) of the drop to its initial diameter (D), was compared to that of the experiment. Table (2) shows the impact conditions for the selected case. Dimensionless time is calculated by using both impact velocity of the drop and the initial diameter of the drop as defined on the axes of Fig. (8). Half of the drop was used for validation simulations along with axisymmetric condition at the central axis of the drop for $2D$ axisymmetric simulations. Different combinations of the viscous flow and contact angle modeling were used to compare the sensitivity of physical phenomena to each method (see Table (3)). Note that the same impact conditions (see Table (2)) are applied to other cases and the differences are coming from viscous flow modeling (laminar/turbulent regime) and wettability approach.

In terms of final outcome, total rebound, partial rebound and deposition was observed for the cases with laminar-SCA, laminar-DCA and turbulent-DCA respectively, although partial rebound was observed in the experiments. This shows the importance of the flow and surface wettability modeling in the balance between inertia, viscous dissipation and surface tension forces which changes the impact outcome drastically from total rebound all the way to deposition. Spread factor is used to compare the experimental results and simulated cases. As it is shown in Fig. (8) the best results are obtained from the simulation case with laminar flow regime and dynamic contact angle to capture the physical aspects of the impact.

To check the consistency of our approach for $3D$ simulations of drop impact on moving walls which is the main purpose of the present work, we validated the same case in $3D$ and a good match was observed as is shown in the same graph. From now on, we use the term "reference case" for the $3D$ validated case.

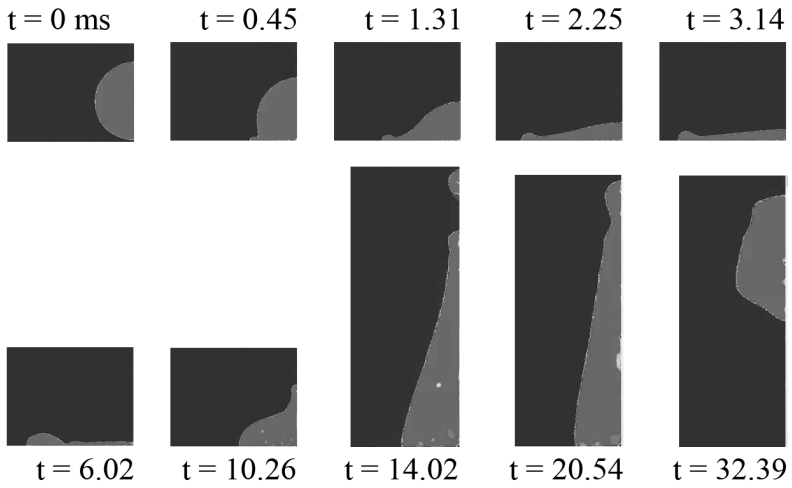

(a) Laminar/SCA

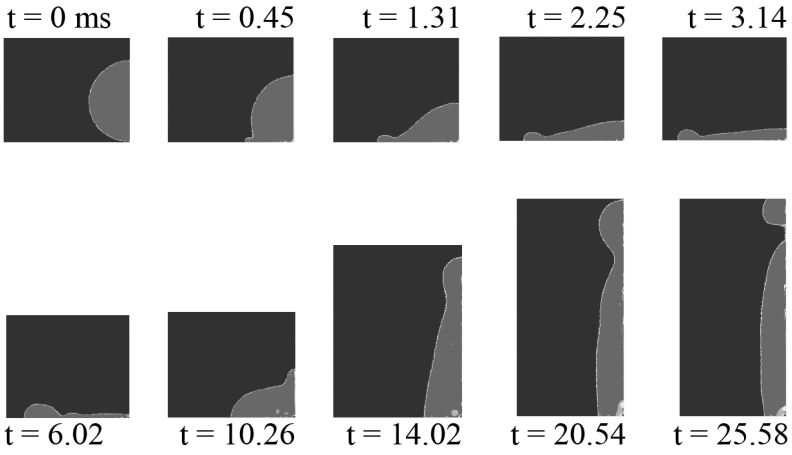

(c) Laminar/DCA

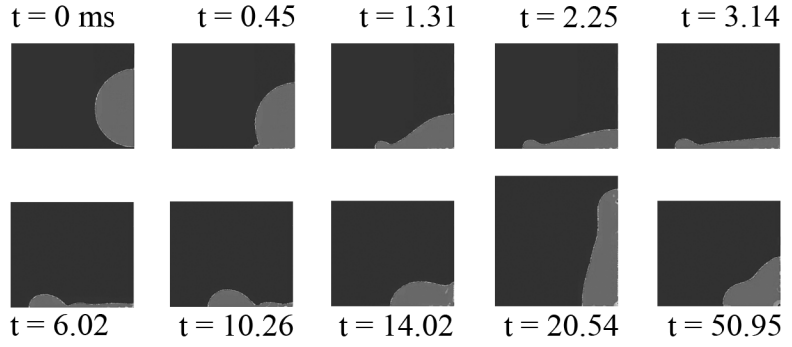

(e) Turbulent/DCA

Figure 7: Time evolution of water drop impact on wax surface. Simulated images are extracted from $2D$ simulation results. Conditions of impact are referenced in Table (2). Time slots are shown in milliseconds. (a)laminar/SCA pair resulted in total rebound (b)laminar/DCA pair resulted in partial rebound (c)turbulent/DCA pair resulted in deposition

Table 2: Impact conditions for the validation case taken from Rioboo et al. [60].

Surface material	Drop diameter (mm)	Impact velocity (m/s)	We	θ°_{adv}	θ°_{rec}
Wax	2.75	1.18	52	105	95

Table 3: Summary of the viscous flow regime and CA modeling approaches for impact on Wax.

Contact angle modeling	θ°_{adv}	θ°_{rec}	θ°_{eq}	We	Viscous flow regime
DCA-Kistler approach	105	95	100	52	Laminar
DCA-Kistler approach	105	95	100	52	Turbulent
SCA	–	–	100	52	Laminar

In both $2D$ and $3D$ cases the results were in good agreement with the experiments both in terms of spread factor matching (see Fig. (8)) and visually (see Fig. (9)). However, to keep this article short, we only present the evolution sequence of the reference case (see Fig. (9)) compared to the experimental results of Rioboo et al. [60].

Analysis of the flow inside the drop (see Fig. (10)) and energy distribution of the competing forces (see Fig. (11)) are more meaningful for the reference case compared to $2D$ axisymmetric one and they reveal insights on such impacts.

Kinetic energy of the drop is calculated based on the velocity of the cells filled with water in our computational domain with the following formula.

$$KE = \int_V (\frac{1}{2}\rho_w \alpha \left(u_x^2 + u_y^2 + u_z^2\right)) \, dV \tag{31}$$

Where u_x, u_y and u_z are components of the velocity vector in x, y and z directions. ρ_w is the density of water. Note that we multiply with volume fraction of water (α) in order to limit our calculation to the liquid phase. The quantity inside the integral shows the energy of the drop per volume of it in which integration would give us finally the kinetic energy associated with the droplet. Potential energy, on the other hand, is calculated based on the normal distance of each grid cell to the wall with the following formula.

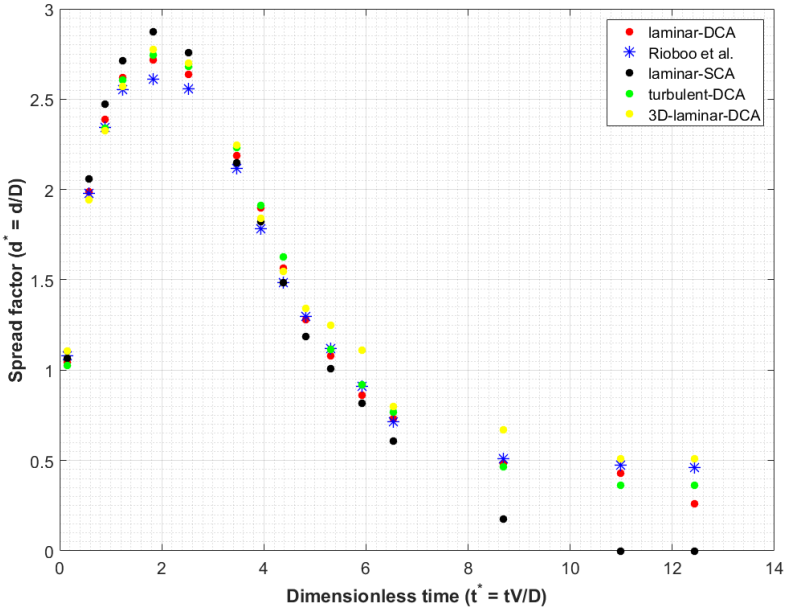

Figure 8: Dimensionless spread factor versus dimensionless time showing the evolution of the spread factor for our reference case.

$$PE = \int_V (\rho_w g h)\, dV \tag{32}$$

Integration of the above quantity on the volume of the drop would give us the potential energy of the drop. Forces regarding surface tension are calculated by considering a constant surface tension (σ) and droplet outer surface (A) in Eq. (33). Here, we take the integral over the outer surface of the drop to obtain the interfacial energy associated with the drop. Viscous dissipations are taken into account as it is shown in Eqs. (34, 35).

$$IE = \int_A \sigma\, dA \tag{33}$$

$$VD = \int_V \mu \alpha \phi_v\, dV \tag{34}$$

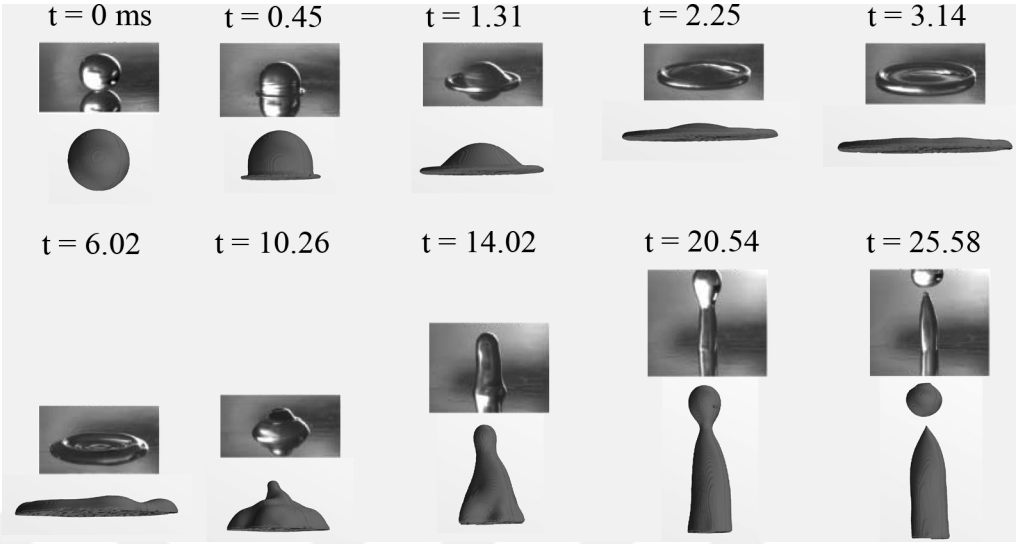

Figure 9: Time evolution of water drop impact on wax surface. Simulated images are extracted from $3D$ simulation results. Conditions of impact are referenced in Table (2). Time slots are shown in milliseconds. Experimental images are taken from Experiments in Fluids, Time evolution of liquid drop impact onto solid, dry surfaces, 33, 2002, pp 112-124, R. Rioboo, M. Marengo and C. Tropea, with permission of Springer.

$$\begin{aligned}\phi_v =& 2\Big[\left(\frac{\partial u_x}{\partial x}\right)^2+\left(\frac{\partial u_y}{\partial y}\right)^2+\left(\frac{\partial u_z}{\partial z}\right)^2\Big]+\left(\frac{\partial u_x}{\partial y}+\frac{\partial u_y}{\partial x}\right)^2+\\ &\left(\frac{\partial u_y}{\partial z}+\frac{\partial u_z}{\partial y}\right)^2+\left(\frac{\partial u_z}{\partial x}+\frac{\partial u_x}{\partial z}\right)^2-\frac{2}{3}\left(\nabla\cdot u\right)^2\end{aligned} \tag{35}$$

We found that the interfacial and kinetic energies are comparable to each other hence in our energy analysis plots we sketched them together on the left axis. The order of potential and viscous dissipation energies are comparable except for the deposition case which we upscaled the viscous dissipations by an order of magnitude. For that reason, potential and viscous dissipation energies are sketched on the right axis of the graphs. Non-dimensionalization of energy levels is done by dividing all energies with the initial kinetic energy of the drop for each case (for impacts on moving surfaces based on values mentioned in Table (4) and for the reference case based on values mentioned in Table (2)).

Figure (11) shows the energy profiles of the $3D$ validated drop impact as a basis

of our work. As it is sketched in the graph, non-dimensional kinetic energy is almost linearly increasing with non-dimensional time till the drop hits the solid wall and the reason for that increase, is clearly because of the effect of gravity. During this time interval interfacial forces (between liquid and gas) are not changing almost, because there is no sign of topological change in the shape of the droplet so that it affects the surface area shared between liquid and gas phases. However, we expect the potential energy of the droplet to drop not only till the impact moment but also a short time after that as well. Since it is calculated for each computational cell with respect to its position to the wall. As the drop spreads over the solid wall we know that the motion is a decelerated motion until the contact line stops its motion and receding stage starts. But, one thing which is interesting here is that there is a short gap between non-moving contact line (non-moving CL) and receding time in which in this period there is not much of a surface area change between phases as the surface forces are not changing. However, kinetic energy is still dropping even after receding stage starts to happen. Looking to Fig. (10) shows that although the drop is not moving its contact line but there are vortex structures activated inside the fluid causing devaluation of kinetic energy at that time. Interfacial force between liquid and gas phases reaches its peak when the drop reaches its maximum spreading diameter which is intuitive because the shared area between them reaches its climax as well. Once retardation of the drop starts, interfacial forces would decrease (reduced shared area) and kinetic energy would increase as a result. Finally, ejection of the secondary drop happens at the second cycle of decline in the kinetic energy. Also, note how presence of vortex structures in the fluid close to the wall (see Fig. (10)) is prohibiting the whole drop to make a total rebound. They start to appear near to the contact line when the drop is in receding phase (at t = 6.02 ms) and grow in number in the vicinity of the wall to help the drop to decrease its momentum resulting attachment of the drop base to the wall.

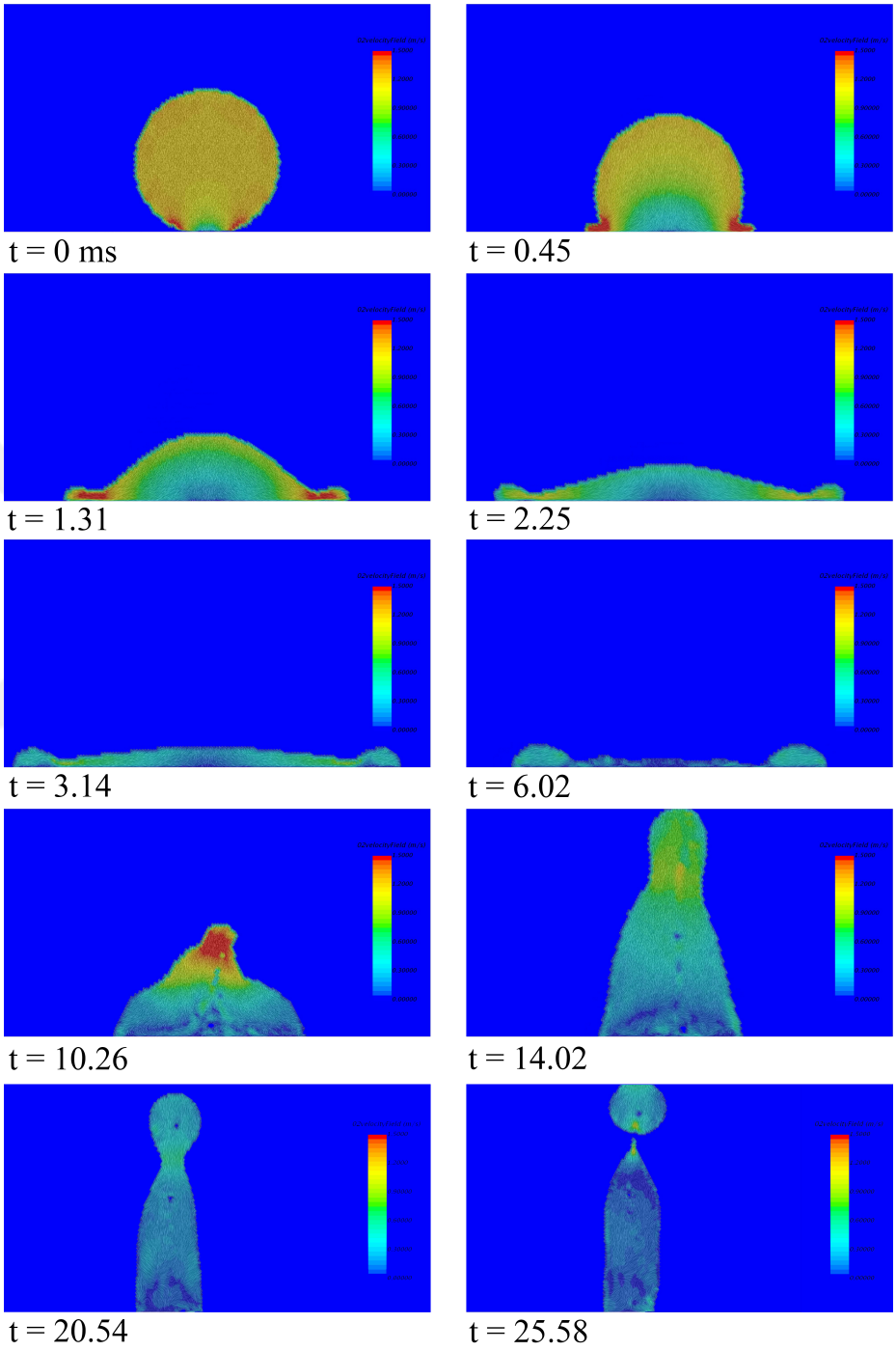

Figure 10: Flow structures inside a drop during impact of the water drop on stationary Wax surface (reference case). Conditions of impact are referenced in Table (2). Time slots are shown in milliseconds.

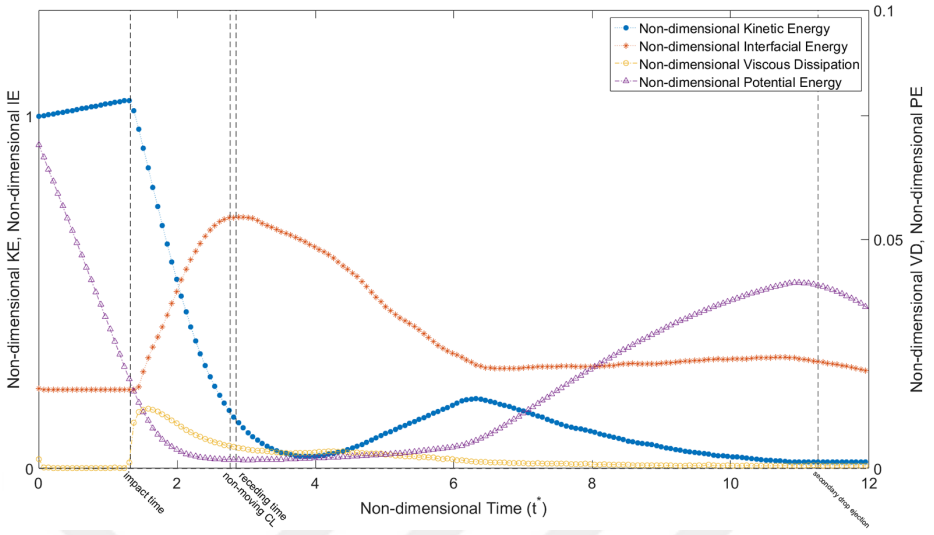

Figure 11: Energy profiles of drop impact on wax surface. Conditions of impact are given in Table 2.

3.4 Conclusion

In this chapter the basis of our numerical scheme in terms of selected models and equations corresponding to those models in which they are going to be solved in Star-CCM+, was presented. Characteristics of the geometry, mesh and boundary conditions were discussed for both $2D$ and $3D$ simulations. The selected case for validation was a water drop impact on a stationary wax surface in which th experimental data of that case was published in the work of Rioboo et al. [60]. Validation was done by comparing time evolution sequence of drop deformation in simulations with obtained images of experiments. Moreover, as a quantitative criterion for validation the spread factor evolution was chased. In a qualitative manner effect of flow and contact angle modeling in three cases of DCA/turbulent, DCA/laminar and SCA/laminar were investigated and resulted in deposition, partial rebound and total rebound which shows a dramatic change in the outcome of drop impact. By monitoring the activities of vortex structures in liquid phase near the wall, this phenomenon was explained as those structures play the role of a prohibiting agent to block the whole drop to make total rebound. Finally, dynamic behaviour of kinetic, interfacial,

potential and viscous dissipation energies were plotted in an energy analysis curve. It was seen that the rate of viscous dissipation increases with much higher slope compared to interfacial energy which shows a smooth behaviour in our graph. However, faster rate does NOT show higher values. In fact, the value associated with interfacial energy is almost and order of magnitude higher than viscous dissipations.

CHAPTER IV

IMPACTS ON MOVING SURFACES

4.1 Problem Statement

In previous chapter the basis of the numerical scheme and its validity for the new simulations which are going to be performed here, were presented through a validation case. In this chapter numerical simulations of the water droplet impact onto a hydrophobic moving surface is going to be investigated. The moving surface is made of Teflon and the key points in which we are going to set the We numbers of the scenario is going to be taken from the work of [11]. Here, since the surface is moving, one clear difference with the previous setup is that not only we are dealing with the We number (ratio of inertial forces to interfacial forces) in normal direction (which is defined by the diameter of the droplet and its velocity) but also another We is defined based on the tangential velocity of the surface and droplet diameter. Outcomes of such impacts are categorized in partial rebound, deposition and split deposition [11] which form a regime diagram shown in Fig. 12. Simulations are defined with one case at each category correspondingly. Detailes of the selected points are presented in a quantitative manner in Table 4.

Table 4: Quantitative representation of selected data points and physical properties of water. Note that subscripts 't' and 'n' stand for tangential and normal components respectively.

Outcome	We_t	We_n	$V_t(m/s)$	$V_n(m/s)$	$D(\mu m)$
Partial rebound	0.3	39.8	0.2	2.4	500
Deposition	5.5	6.7	0.9	1	500
Split deposition	149	42.3	4.7	2.5	500

Liquid	Density (kg/m^3)	Viscosity $(mPa.s)$	Surface tension (N/m)
Water	998	0.98	0.074

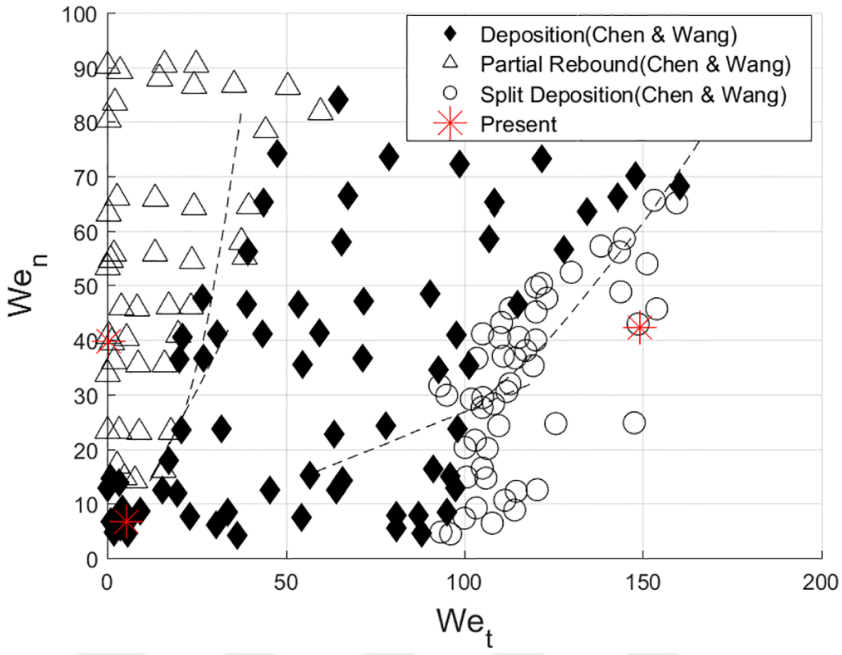

Figure 12: Outcomes of water droplet impacts on Teflon surface. Red asterisks are representing the selected computational data points in a qualitative manner.

4.2 Numerical Setup

Three dimensional ($3D$) simulations of drop impact on moving walls were done for partial rebound, deposition and split deposition regimes. Deposition and split deposition cases were solved with a workstation equipped with Intel(R) Xeon(R) CPU E5-26600 consisting of 16 cores (32 logical processors) and 64.0 GB of RAM. However, for partial rebound scenario we had to used two of the same workstations through MPI capability available in StarCCM+, since we were dealing with more computational cells. All information regarding the numerical setup for the simulations in this chapter can be found in detail in 3.2.

4.2.1 Computational Domain

Computational domains that we used for different cases were all a rectangular cuboid (see Fig. (13)) but with different sizes and consequently different mesh resolutions (see Table (5)). We picked the size of our domains based on the time scales for an

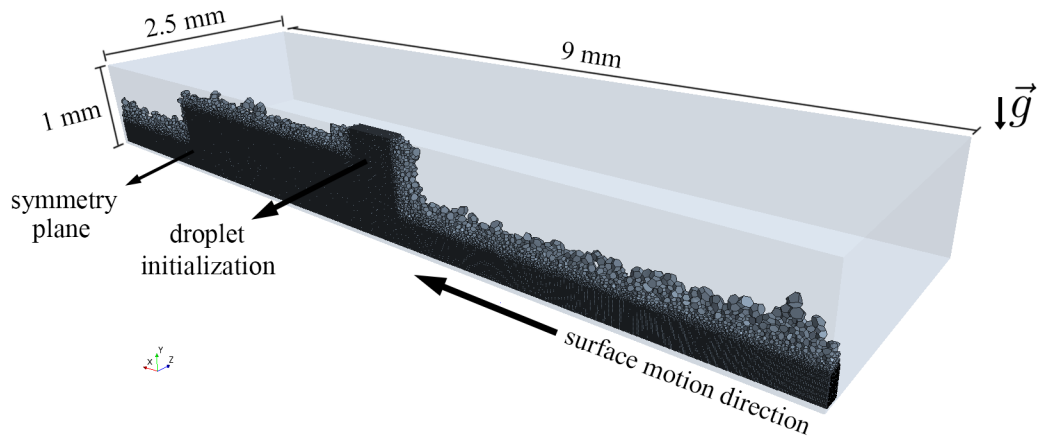

Figure 13: A sample of the computational domain and mesh structure in the refined areas. This configuration is specifically for the case of partial rebound (see Table (4)).

Table 5: Geometric properties and grid resolution for different impact conditions.

Case	Droplet size	Domain size[1]	No. of grid cells
Partial rebound	$500\,\mu m$	$9 \times 1 \times 2.5$	≈ 30 million
Deposition	$500\,\mu m$	$9 \times 1 \times 2.5$	≈ 8 million
Split deposition	$500\,\mu m$	$19 \times 1 \times 1.5$	≈ 13 million
$3D$ Validation	$2.75\,mm$	$10 \times 7 \times 9$	≈ 3 million
$2D$ Axisymmetric validation	$2.75\,mm$	2×6	≈ 51000

impact scenario to take place combined with the velocities of the droplet and wall. Figure 5 also provides information on the size of our computational domains.

4.2.2 Boundary Conditions

Boundary conditions for these simulations were quite similar to the previous chapter with differences mentioned in this part. In all outer surfaces of the cuboid, the pressure outlet boundary condition was selected except the one at the bottom on which the wall condition was implemented and the one at the front in which the symmetry condition was applied. The value of $0\,Pa$ was entered for the pressure outlet condition with respect to the ambient atmospheric pressure. For the wall, no-slip boundary condition was picked and depending on the DCA or SCA the advancing and receding contact angles or static contact angle was selected, respectively. These

values for the case of water droplet on Teflon surface were taken from Ruiz-Cabello et al. [63]. Other than contact angle values, the other condition which was different from the previous chapter simulations was adding a tangential velocity component for the wall. Information about different tangential velocities for each impact scenario can be found in Table 4.

4.2.3 Mesh Properties

Polyhedral mesh was used to mesh the computational domain. And, depending on the size of the domain, the number of cells were different. The resolution for the cases of deposition and split deposition was more or less the same however, we used better resolution for partial rebound case in order to capture the correct physical behaviour in our simulations. Trajectory of the droplet while it is moving towards the surface and also a specific thickness from the wall were resolved more by using custom control mesh size capability in Star-CCM+. The closest distance from the wall for deposition and split deposition cases that we could resolve was 5 μm while this value decreased to 1 μm for the case of partial rebound. A sample of the refined regions in our partial rebound case can be seen in Fig. 13. More information on the number of cells for each case is given in Table 5.

4.3 Results and Discussion

Evolution sequence of different impact scenarios for the case of Laminar-DCA is depicted in Fig. (4.3). In the first scenario (Fig. 14(a)), drop hits the surface, spreads over, reaches to its maximum spreading diameter, then starts receding and finally while a small portion of it, is attached to the surface a big portion disassembles from it which makes what is called as partial rebound in literature. In the second one (Fig. 14(b)), after drop hits the surface, it will spread over and simply retards and deposits on the wall which makes what is called deposition in literature. And, in final case (Fig. 14(c)), high velocity of the wall makes more extension in the direction

of surface motion. Then, bubble entrapment (which its presence has been shown in experimental work of Mehdi-Nejad et al. [44] and also in simulations of Heidarifatasmi and Ertunç [27]) causes the first rupture of the drop ($t = 0.75\,ms$). Later, because of high tangential velocity of the wall the trail of the drop detaches ($t = 1.4\,ms$) which makes what is called as split deposition in available literature.

Figure 15 shows the evolution sequence of bubble entrapment at the central plane of the spreading droplet. The drop almost sits over the surface (at $t = 0.20\,ms$) and the pressurized entrapped air has almost diameter of $8\mu m$ which starts to move in the direction of surface motion (at $t = 0.24, 0.29$ and $0.33\,ms$). Looking into central plane, one would assume that the first splitting happens at $t = 0.37\,ms$ where there is no connection between the small portion and the rest of the droplet. But in fact it shows that the bubble could rupture the central surface of the droplet and this can be clearly seen by looking into evolution sequence of split deposition at instance of $0.4\,ms$. Then, almost at the beginning of receding, the entrapped bubble can overcome the force created by surface tension and makes the first splitting (at $t = 0.75\,ms$).

Outcomes of the simulations are matching with the outcomes of the experimental tests done by Chen and Wang [11]. If we compare the reference case with the partial rebound on moving walls, a big portion of the drop is attached to the surface while a small portion detaches from the drop in case of reference case, on contrary due to the surface motion and its effect on internal vortices of the drop only a small portion is attached to the wall while a big portion separates.

Energy profiles for selected cases of partial rebound, deposition and split deposition are shown in Fig. (4.3). Looking into Fig. (16(a)) which is for partial rebound case, first cycle for KE is due to the nature of the dynamics of impact and is present in both impacts on stationary and moving ones. However, one would expect normally an increase in KE due to the surface motion but there is no sign of such trend simply because the area of contact (after secondary drop ejection) between the drop

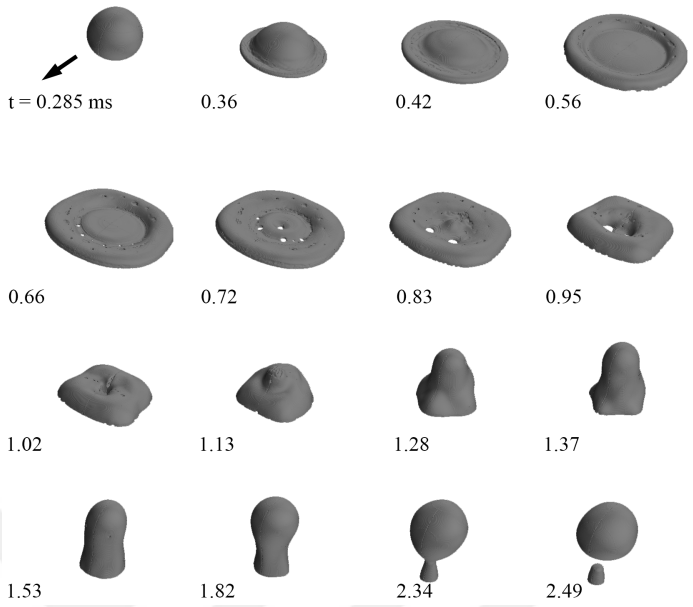

(a) Partial rebound

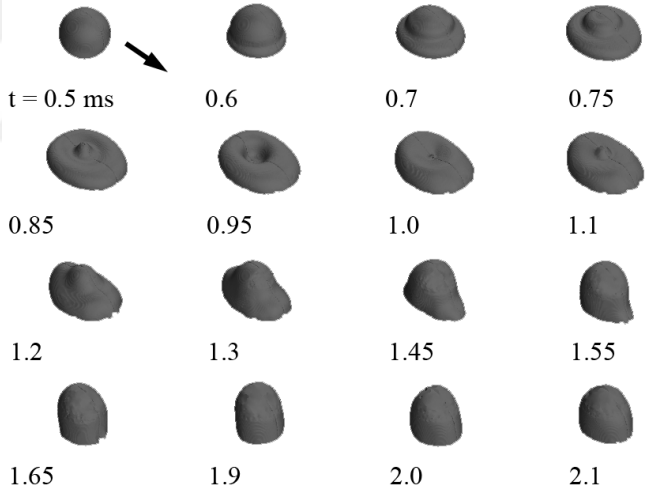

(c) Deposition

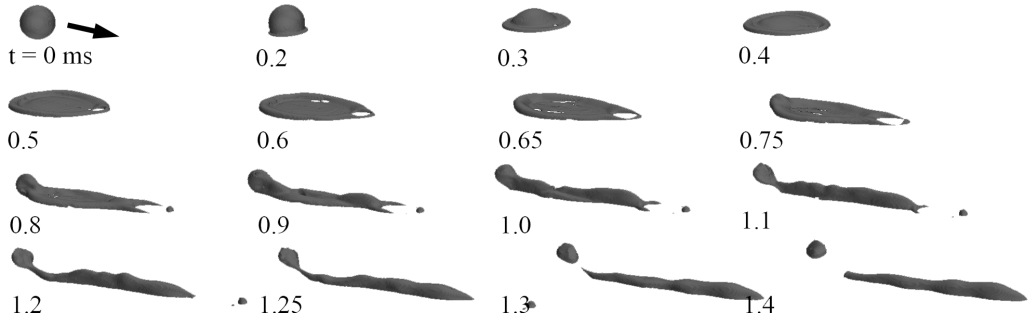

(e) Split deposition

Figure 14: Time evolution of water drop impacting on a moving hydrophobic wall (Teflon) obtained from 3D simulations. (a) $We_n = 39.8, We_t = 0.3$ (b) $We_n = 6.7, We_t = 5.5$ (c) $We_n = 42.3, We_t = 149$.

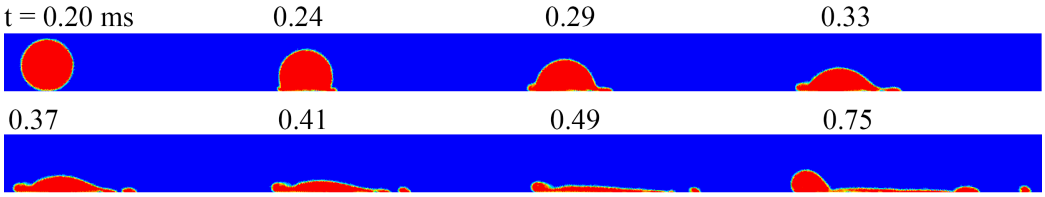

Figure 15: Evolution and motion of entrapped bubble in case of split deposition. Volume fraction instances are shown at the central plane of the droplet.

and surface is very small at later stages as it is shown in Fig. (14(a)). Considering interfacial forces one can understand almost in all cases, the drop more or less ends up with a constant area which results in a plateau at final stages of impact. The behavior of PE is fairly straight forward for all considered cases and only in partial rebound cases we see a sharp difference between the least amount of PE (at maximum drop spreading) and its final value just a bit after secondary drop ejection which is caused by the nature of partial rebound where the drop extends its surface area in vertical direction.

Second plot (see Fig. 16(b)) shows the impact conditions regarding the deposition case in which KE is not going to fade away at final stages of this phenomenon but it starts to increase with a slight slope. The reason of such behavior comes with the velocity of the surface and impact velocity of the drop which they are almost equal to each other (see Table (4). The portion of the drop which is moving in the same direction with the surface will have increased velocity while wall prohibits the other portion which is moving in the opposite direction with respect to the surface motion. And since they have almost the same velocity the increase in KE is not significant after the second cycle of KE curve. Note that presence of second cycle in KE happens only for deposition and split deposition cases.

The third case (see Fig. 16(e)) which corresponds to the split deposition impact conditions, shows a sharp increase in KE curve after impact, however, this does not mean that the first cycle is going to be removed. However, the duration for second

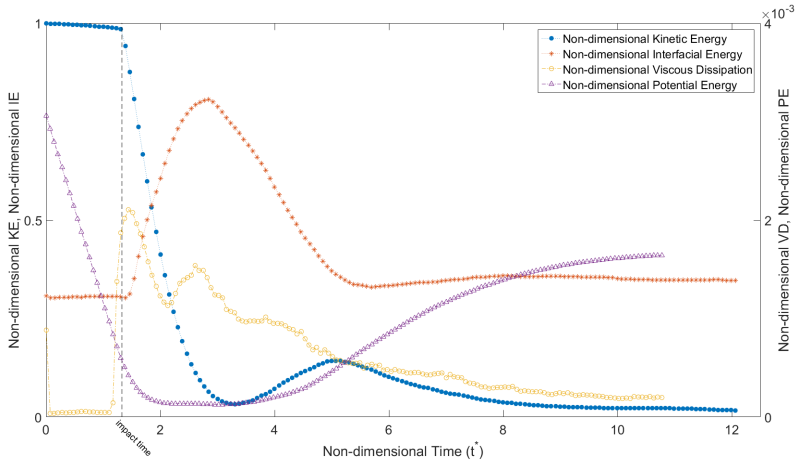

(a) Partial rebound

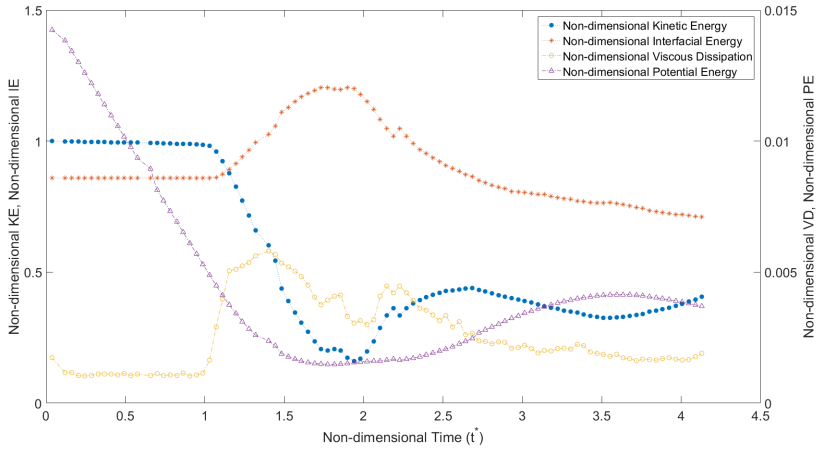

(c) Deposition

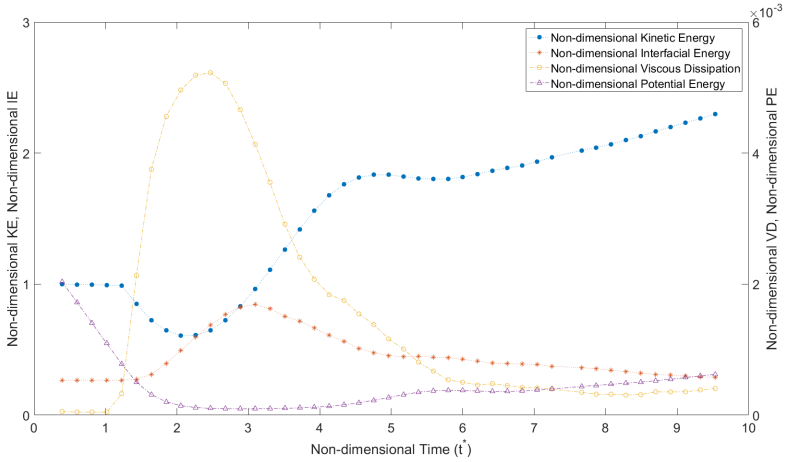

(e) Split deposition

Figure 16: Time evolution of water drop impacting on a moving hydrophobic wall (Teflon) obtained from 3D simulations. (a) $We_n = 39.8, We_t = 0.3$ (b) $We_n = 6.7, We_t = 5.5$ (c) $We_n = 42.3, We_t = 149$.

cycle in KE is much shorter in split deposition compared to deposition case because of high inertia coming from surface motion.

Our results are showing that topological changes of the surface of the drop is poorly affected by the wall velocity since for the partial rebound and split deposition cases the normal velocities are almost the same and the only significant difference comes from the tangential velocity of the wall. For both cases the maximum surface area happens almost in the same dimensionless time ($t^* = 3.0$). Surface velocity shows itself in shifting the KE curve to the left as it can be seen from Fig. (4.3). In other words, it generates a time lag between the interfacial and inertial forces in the dynamics of the drop impacts. A physical explanation for such behavior can be inferred by looking into dimensionless viscous dissipation curves of partial rebound and split deposition cases. High shear due to high surface motion creates a spike in dimensionless viscous dissipation from 0.53 (partial rebound) to 2.61 (split deposition). This makes the kinetic energy to drop to its minimum for both cases only with the difference that the minimum of KE in split deposition is higher than the one in partial rebound.

It is clear that in case of moving surfaces the drop is going to spread in an oval shape instead of a circular one and the ratio of the bigger diameter (b) to the smaller one (d_m) at maximum drop spreading, is represented by γ_A which is almost constant in two possible conditions as stated in [11]. For both deposition and partial rebound regimes this ratio is equal to 1.1 (in experiments) and in case of split deposition this value increases to 1.46 while the results of our simulations are showing 1.05 for the case of partial rebound, 1.04 for case of deposition and 1.6 for split deposition case (see Fig. 17).

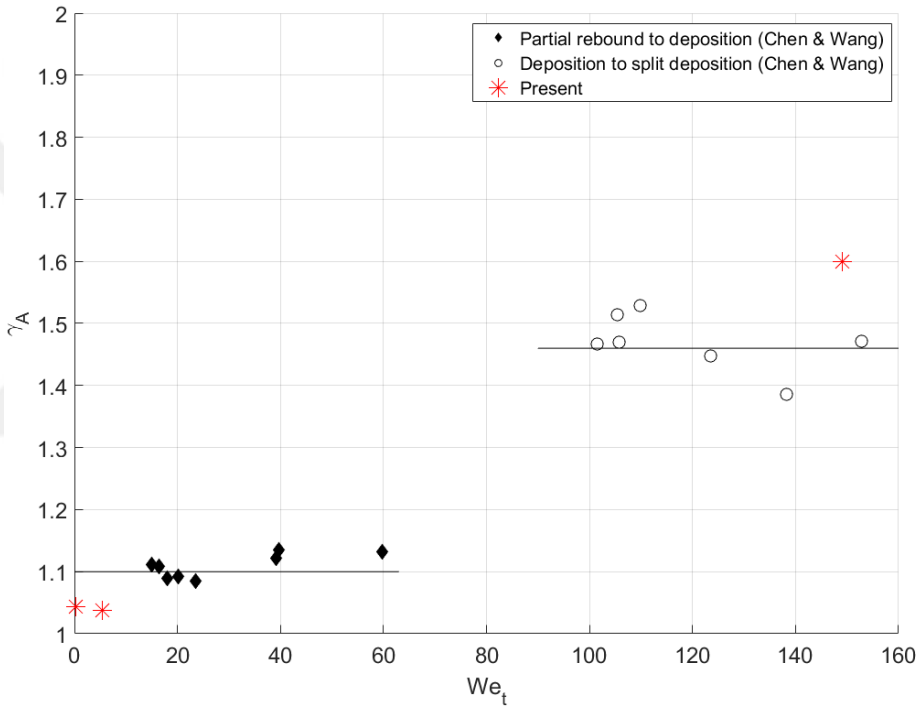

Figure 17: Ratio of diameters at maximum drop spreading. For partial rebound and deposition this ratio is 1.1 ($\gamma_A = 1.1$) while it increases to 1.46 ($\gamma_A = 1.46$) for case of split deposition. Experiments are done by R. H. Chen, H. W.Wang, Experiments in Fluids, 39, 754(2005). Red asterisks are showing simulation results.

4.4 Conclusion

In this chapter the same numerical approach which was discussed in detail before, was used in order to study impacts of water droplets on hydrophobic moving walls. Characteristics of the geometry, mesh and boundary conditions were presented for our numerical simulations. Impact scenarios were containing partial rebound, deposition and split deposition outcomes out of impacts of water droplets on Teflon surface as it was documented in [11]. Time evolution of such impacts were presented along with description of each impact scenario. Ratio of the bigger droplet diameter to the smaller one at maximum drop spreading (γ_A) was calculated for all three cases of impact and compared with experimental results of [11] in which the results were within 10% of relative error with respect to experimental values. Finally, dynamic behaviour of kinetic, interfacial, potential and viscous dissipation energies were plotted in an energy analysis curve for each case. Dealing with the case of water drop impact on stationary solid surface we had a sudden spike for viscous dissipation at the moment of impact however, in case of moving walls it starts to increase slightly before impact. This clearly shows the shear caused by air boundary layer. Another difference is that when maximum drop spreading (maximum peak in interfacial energy curve) happens in case of stationary wall, we still have decreasing trend for kinetic energy (until it reaches to its minimum point) in which we related that effect to the activation of viscous dissipation through vortices. While, tangential velocity component of the surface can provoke existence of minimum kinetic energy by the time the drop is still stretching its outer surface.

CHAPTER V

CONCLUSION AND FUTURE WORK

Two and three dimensional simulations of droplet impacts on solid surfaces have been done for static and moving walls. In $2D$ static wall simulations, it is shown that different viscous flow and contact angle models cause a forceful change in the outcome of the drop impact from total rebound to deposition. Moving to three dimensional simulations, prevention of a total rebound in presence of vortex structures in liquid close to the wall was shown for our reference case. In fact, their presence was also concluded by looking at the energy profiles in the region of non-moving CL and receding time, as a reducing mechanism for kinetic energy of the drop. Such structures can create a time lag between the interfacial and inertial dynamics of the drop impacts.

In $3D$ moving wall simulations, all regimes found in the regime diagram of Chen and Wang [11], namely deposition, partial rebound and split deposition, can be simulated with the numerical approach implemented in this work. In split deposition case, the role of bubble entrainment in rupturing and splitting was mentioned.

We analyzed the evolution of droplet's potential, kinetic, interfacial and dissipated energy. It is shown that viscous dissipation starts to increase slightly before impact and it shows a sudden increase upon impact in the kinematic phase. In general, the kinetic energy drops first due to dissipation and surface enlargement and, in later stages, it increases as a result of surface motion and retraction. Counter intuitively, as the tangential We is increased, the viscous dissipation attains higher value and shifts the minimum of kinetic energy profile to an earlier dimensionless time but with a higher value. It is found that the dimensionless time where maximum spread of the

droplet happens is less influenced by tangential We number.

For future work, one can consider the dynamic behaviour of entrapped bubble for the case of droplet impacts on moving walls to explain how the entrapped bubble is able to rupture the drop. Superhydrophobic surfaces has gained importance in recent years which means innovative ideas regarding such surfaces can be investigated numerically. Moreover, impacts on vibrating surfaces has attracted the attentions recently and preliminary experimental studies have been done already by researchers. This can open doors to more deep investigations in this category of drop impacts. Also, there are always novel ideas and new configurations for drop impacts to consider specially the ones with their potential applications in spray systems. Finally, For each impact scenario care must be taken to analyze the flow structures within the liquid instead of looking at external factors which might affect those impacts.

APPENDIX A

SOME ANCILLARY STUFF

A.0.1 MATLAB Script For Hoffman Function Calculation

MATLAB code to calculate and show the difference between the dynamic contact angle values (advancing and receding) with the static contact value. Value of capillary number is taken from the simulations.

```
close all
clear all
thetaAdvancing = 141 * pi / 180; % converting to radians
thetaReceding = 81 * pi / 180; % converting to radians
Ca = 0.083758;
Caeq = 0.001;
% using syms form (symbolic expression) to calculate the inverse of Hoffman % function.
syms theta;
% hoffman = inline( 'acos(1 - 2 * tanh(5.16 * (theta / (1 + 1.31 * theta ^ 0.99))^0.706))' );
hoffman = symfun(acos(1 - 2 * tanh(5.16 * (theta / (1 + 1.31 * theta ^ 0.99))^0.706)), theta);
% hoffmanInverse = finverse(hoffman);
%% taking the inverse of the function by hand and putting the function in this section.
a =symfun(( (1/5.16) * atanh(0.5 * (1 - cos(theta))) )^(1 / 0.706), theta);
hoffmanInverse = symfun(a / (1 - 1.31 * a), theta);
```

```
% this section is for advancing contact angle changes
dynamicCA = zeros(1, 8);
CaCounter = zeros(1, size(dynamicCA, 2));
CaCounter(1, 1) = Ca;
for i = 1:8
T = eval(hoffmanInverse(thetaAdvancing));
kistlerTheta = eval(hoffman(Ca + T));
dynamicCA(1, i) = kistlerTheta * 180 / pi;
Ca = Ca - 0.01;
CaCounter(1, i) = Ca;
end
h(1) = scatter(CaCounter, dynamicCA, 100, 'k', 'filled');
hold on
scatter(0, 141, 100, 'k', 'filled');
% this section is for receding contact angle changes
% initializing the variables to their initial value
Ca = 0.083758;
dynamicCA = zeros(1, 8);
CaCounter = zeros(1, size(dynamicCA, 2));
CaCounter(1, 1) = Ca;
for i = 1:8
T = eval(hoffmanInverse(thetaReceding));
kistlerTheta = eval(hoffman(Ca + T));
dynamicCA(1, i) = kistlerTheta * 180 / pi;
Ca = Ca - 0.01;
CaCounter(1, i) = Ca;
end
```

```
h(2) = scatter(CaCounter, dynamicCA, 100, 'r', 'filled');
scatter(0, 81, 100, 'r', 'filled');
% axis settings
xlabel('Capillary number', 'FontSize', 15);
ylabel('Contact Angle (^\circ)', 'FontSize', 15);
set(gca, 'FontSize', 15);
grid on
% adding static contact angle
CaCounter2 = zeros(1, size(CaCounter, 2) + 1);
CaCounter2(1, 1) = 0;
for i = 2: size(dynamicCA, 2) + 1
CaCounter2(1, i) = CaCounter(1, i - 1);
end
h(3) = plot(CaCounter2, 103 * ones(1, size(dynamicCA, 2) + 1) , 'b', 'LineWidth',
2);
% legend settings
leg = legend(h(1:3), 'Advancing contact angle', 'Receding contact angle', 'Equi-
librium contact angle');
leg.FontSize = 15;
hold off
%% For stability section
% if (Ca < Caeq) && (Ca > -Caeq)
% f = 0.5 + 0.5 * cos( (Ca / Caeq) * pi);
% dynamicTheta = f * thetaEquilibrium + (1 - f) * kistlerTheta;
% end
```

A.0.2 MATLAB Script For Video Generation

MATLAB code for video making out of series of images with a static name plus a dynamic number assigned:

```
clear all
close all
% creating a video object and writing onto it
outputVideo = VideoWriter('vibrating4000hzVelConvExtDom.avi');
outputVideo = VideoWriter('vibrating4000hzExtDom.avi');
outputVideo.FrameRate = 23.976;
open(outputVideo)
for i = 15 :15 : 8550
img = imread(sprintf('waterVolFrac_image_%05d.png', i));
imshow(img)
drawnow
currentFrame = getframe;
writeVideo(outputVideo, currentFrame)
end
close(outputVideo)
% view the final video file created.
dropVideo = VideoReader('vibrating4000hzExtDom.avi');
i = 1;
while hasFrame(dropVideo)
mov(i) = im2frame(readFrame(dropVideo));
i = i + 1;
end
% setting the figure properties for showing the video in the same size as
% the video width and height.
```

```
f = figure;
f.Position = [150 150 dropVideo.Width dropVideo.Height];
ax = gca;
ax.Units = 'pixels';
ax.Position = [0 0 dropVideo.Width dropVideo.Height];
image(mov(1).cdata,'Parent',ax)
axis off
movie(mov, 1, dropVideo.FrameRate)
```

A.0.3 JAVA Script For Star-CCM+

Java code for StarCCM+ in order to extract some useful data:

```
// STAR-CCM+ macro: historyDataExtraction01.java
// Written by STAR-CCM+ 10.06.010
package macro;
import java.util.*;
import star.common.*;
import star.base.neo.*;
import star.base.report.*;
import star.post.*;
import java.io.BufferedWriter;
import java.io.File;
import java.io.FileWriter;
import java.io.IOException;
import star.base.report.Report;
import star.base.report.VolumeIntegralReport;
public class historyDataExtraction01 extends StarMacro {
public void execute() {
```

```
execute0();
}
private void execute0()  {
Simulation simulation_0 = getActiveSimulation();
SolutionHistory solutionHistory_0=simulation_0.get(SolutionHistoryManager.class
).createForFile(resolvePath("D:\\simulations\\validation\\historyFiles\\2\\hist-
ory00.simh"), true);
RecordedSolutionView recordedSolutionView_0 = solutionHistory_0.createRecord-
edSolutionView();
VolumeIntegralReport volumeIntegralReport_0 = ((VolumeIntegralReport) simu-
lation_0.getReportManager().getReport("kineticEnergy"));
Region region_0 = simulation_0.getRegionManager().getRegion("Region");
volumeIntegralReport_0.getParts().setObjects(region_0);
VolumeIntegralReport volumeIntegralReport_1 = ((VolumeIntegralReport) simu-
lation_0.getReportManager().getReport("potentialEnergy"));
volumeIntegralReport_1.getParts().setObjects(region_0);
VolumeIntegralReport volumeIntegralReport_2 = ((VolumeIntegralReport) simu-
lation_0.getReportManager().getReport("viscousDissipation"));
volumeIntegralReport_2.getParts().setObjects(region_0);
SolutionRepresentation solutionRepresentation_0 = ((SolutionRepresentation) sim-
ulation_0.getRepresentationManager().getObject("history00"));
volumeIntegralReport_0.setRepresentation(solutionRepresentation_0);
volumeIntegralReport_1.setRepresentation(solutionRepresentation_0);
volumeIntegralReport_2.setRepresentation(solutionRepresentation_0);
int timeStepCounter = 1;
for (int i = 1 ; i <= 225 ; i++){
String dirName = "D:\\simulations\\javaDumbFileTest\\newSet\\";
```

```
String fileName = "timeStep_" + timeStepCounter + ".csv";
File dir = new File (dirName);
File file = new File(dir, fileName);
Collection <Report>  reps = simulation_0.getReportManager().getObjects();
try {
BufferedWriter out = new BufferedWriter(new FileWriter(file));
out.append("Report Name, Report Value");
out.newLine();
for(Report ri : reps) {
if(ri instanceof VolumeIntegralReport){
VolumeIntegralReport vr = (VolumeIntegralReport) ri;
out.append(vr.getPresentationName() + ", " + vr.getValue());
out.newLine(); } out.close();
}
catch (IOException ex) {
simulation_0.println("Error type:" + ex.getMessage());
}
timeStepCounter = timeStepCounter + 20;
recordedSolutionView_0.setStateName("State " + timeStepCounter);
// printing in each 5 timesteps the output of the reports.
//volumeIntegralReport_0.printReport();
//volumeIntegralReport_1.printReport();
volumeIntegralReport_2.printReport();
}
}
}
```

A.0.4 JAVA Script For Adaptive Meshing

```
// STAR-CCM+ macro: adaptiveMesh.java
    // Written by STAR-CCM+ 10.06.010
    // here I'm tryin to make a new .java file for the simulations capable of changing the mesher table at the initialization step and then when we start the simulation. Also I need to find out with the new dimension set how should I update the adaptive mesh so that it would be almost an optimum case for us.
    package macro;
    import java.util.*;
    import star.common.*;
    import star.base.neo.*;
    import star.meshing.*;
    import star.vis.*;
    import star.twodmesher.*;
    public class adaptiveMeshAdvanced3 extends StarMacro {
    public void execute() {
    execute0();
    }
    private void execute0() {
    int counter = 1;
    int timeStepCounter = 5;
    Simulation simulation_0 = getActiveSimulation();
    Scene scene_0 = simulation_0.getSceneManager().getScene("volGrad");
    Scene scene_1 = simulation_0.getSceneManager().getScene("waterVolFrac");
    Scene scene_2 = simulation_0.getSceneManager().getScene("VolFracWithoutMesh");
    MeshPipelineController meshPipelineController_0 = simulation_0.get(MeshPipeline-
Controller.class);
```

```
simulation_0.getSimulationIterator().step(1);
XyzInternalTable xyzInternalTable_0 = ((XyzInternalTable) simulation_0.getTable-
Manager().getTable("meshRefinementTable"));
xyzInternalTable_0.extract();
meshPipelineController_0.generateVolumeMesh();
// stepping 5 times for the first time
simulation_0.getSimulationIterator().step(5);
counter = 1;
for (;counter  <  5; counter++){
// inside the loop instructions.
// first extract the table for the mesh refinement at the interface.
xyzInternalTable_0.extract();
meshPipelineController_0.generateVolumeMesh();
// stepping 5 times
simulation_0.getSimulationIterator().step(5);
// updating the timeStepCounter
timeStepCounter = timeStepCounter + 5;
// taking volGrad and volFrac data
// volGrad scene settings
CurrentView currentView_0 = scene_0.getCurrentView();
currentView_0.setInput(new DoubleVector(new double[ ] -7.512932856588267E-4,
0.0037112011592631165, -0.004820509867870547), new DoubleVector(new double[ ]
-7.512932856588267E-4, 0.0037112011592631165, 0.015563067925966047), new Dou-
bleVector(new double[ ] 1.0, 0.0, 0.0), 0.00532118158650138, 0);
scene_0.printAndWait(resolvePath("D:\\simulations\\adaptiveMesh\\volGrad\\-
volGrad" + timeStepCounter + ".png"), 1, 1322, 653);
// volFrac scene settings
```

```
CurrentView currentView_1 = scene_1.getCurrentView();
currentView_1.setInput(new DoubleVector(new double[ ] -7.512932856588267E-4,
0.0037112011592631165, -0.004820509867870547), new DoubleVector(new double[ ]
-7.512932856588267E-4, 0.0037112011592631165, 0.015563067925966047), new Dou-
bleVector(new double[ ] 1.0, 0.0, 0.0), 0.00532118158650138, 0);
scene_1.printAndWait(resolvePath("D:\\simulations\\adaptiveMesh\\volFrac\\-
volFrac" + timeStepCounter + ".png"), 1, 1322, 653);
CurrentView currentView_2 = scene_2.getCurrentView();
currentView_2.setInput(new DoubleVector(new double[ ] -7.512932856588267E-4,
0.0037112011592631165, -0.004820509867870547), new DoubleVector(new double[ ]
-7.512932856588267E-4, 0.0037112011592631165, 0.015563067925966047), new Dou-
bleVector(new double[ ] 1.0, 0.0, 0.0), 0.00532118158650138, 0);
scene_2.printAndWait(resolvePath("D:\\simulations\\adaptiveMesh\\volFracW-
ithoutMesh\\volFrac" + timeStepCounter + ".png"), 1, 1322, 653);
}
counter = 1;
}
}
```

Bibliography

[1] Thomas A Baer, Richard A Cairncross, P Randall Schunk, P A Sackinger, and Rekha R Rao. A finite element method for free surface flows of incompressible fluids in three dimensions. {Part II}: dynamic wetting line. *Int. Jour. Num. Meth. Fluids*, 33(June 1999):405–427, 2000.

[2] H. Bararnia, S.M. Seyyedi, D.D. Ganji, and B. Khorshidi. Numerical investigation of the coalescence and breakup of falling multi-droplets. *Colloids and Surfaces A: Physicochemical and Engineering Aspects*, 424:40–51, may 2013. ISSN 09277757. doi: 10.1016/j.colsurfa.2013.02.024. URL http://linkinghub.elsevier.com/retrieve/pii/S0927775713001271.

[3] James C. Bird, Scott S H Tsai, and Howard a. Stone. Inclined to splash: Triggering and inhibiting a splash with tangential velocity. *New Journal of Physics*, 11, 2009. ISSN 13672630. doi: 10.1088/1367-2630/11/6/063017.

[4] Edward Bormashenko. Why does the Cassie-Baxter equation apply? *Colloids and Surfaces A: Physicochemical and Engineering Aspects*, 324(1-3):47–50, 2008. ISSN 09277757. doi: 10.1016/j.colsurfa.2008.03.025.

[5] J. U. Brackbill, D. B. Kothe, and C. Zemach. A continuum method for modeling surface tension. *Journal of Computational Physics*, 100(2):335–354, 1992. ISSN 10902716. doi: 10.1016/0021-9991(92)90240-Y.

[6] Simon Brandon, Nir Haimovich, Einat Yeger, and Abraham Marmur. Partial wetting of chemically patterned surfaces: The effect of drop size. *Journal of Colloid and Interface Science*, 263(1):237–243, 2003. ISSN 00219797. doi: 10.1016/S0021-9797(03)00285-6.

[7] M. Bussmann, J. Mostaghimi, and S. Chandra. On a three-dimensional volume tracking model of droplet impact. *Physics of Fluids*, 11 (6):1406, 1999. ISSN 10706631. doi: 10.1063/1.870005. URL http://scitation.aip.org/content/aip/journal/pof2/11/6/10.1063/1.870005.

[8] Richard A. Cairncross, P. Randall Schunk, Thomas A. Baer, Rekha R. Rao, and Phillip A. Sackinger. A finite element method for free surface flows of incompressible fluids in three dimensions. part i. boundary fitted mesh motion. *International Journal for Numerical Methods in Fluids*, 33(3):375–403, 2000. ISSN 1097-0363. doi: 10.1002/1097-0363(20000615)33:3¡375::AID-FLD13¿3.0.CO;2-O. URL http://dx.doi.org/10.1002/1097-0363(20000615)33:3<375::AID-FLD13>3.0.CO;2-O.

[9] A. B. D. Cassie and S. Baxter. Wettability of porous surfaces. *Transactions of the Faraday Society*, 40(5):546, 1944. ISSN 0014-7672. doi: 10.1039/tf9444000546. URL http://xlink.rsc.org/?DOI=tf9444000546.

[10] Rajib Ghosh Chaudhuri and Santanu Paria. Journal of Colloid and Interface Science Dynamic contact angles on PTFE surface by aqueous surfactant solution in the absence and presence of electrolytes. *Journal of Colloid And Interface Science*, 337(2):555–562, 2009. ISSN 0021-9797. doi: 10.1016/j.jcis.2009.05.033. URL `http://dx.doi.org/10.1016/j.jcis.2009.05.033`.

[11] R. H. Chen and H. W. Wang. Effects of tangential speed on low-normal-speed liquid drop impact on a non-wettable solid surface. *Experiments in Fluids*, 39: 754–760, 2005. ISSN 07234864. doi: 10.1007/s00348-005-0008-6.

[12] Emil Chibowski and Konrad Terpilowski. Surface free energy of sulfur-Revisited. I. Yellow and orange samples solidified against glass surface. *Journal of Colloid and Interface Science*, 319(2):505–513, 2008. ISSN 00219797. doi: 10.1016/j.jcis.2007.10.059.

[13] G E Cossali, A Coghe, and M Marengo. The impact of a single drop on a wetted solid surface, 1997. ISSN 0723-4864.

[14] G. E. Cossali, M. Marengo, a. Coghe, and S. Zhdanov. The role of time in single drop splash on thin film. *Experiments in Fluids*, 36(6):888–900, 2004. ISSN 07234864. doi: 10.1007/s00348-003-0772-0.

[15] R. G. Cox. The dynamics of the spreading of liquids on a solid-surface .1. viscous-flow. *J. Fluid Mech.*, 168(April 2006):169–194, 1986. ISSN 0022-1120. doi: 10.1017/S0022112086000332.

[16] Jacques Désarménien. How to run TEX in french. Technical Report SATN-CS-1013, Computer Science Department, Stanford University, Stanford, California, August 1984.

[17] E B Dussan. On the Spreading of Liquids on Solid Surfaces: Static and Dynamic Contact Lines. *Annual Review of Fluid Mechanics*, 11(1):371–400, 1979. ISSN 0066-4189. doi: 10.1146/annurev.fl.11.010179.002103.

[18] Saeed Fathi, Phill Dickens, and Farid Fouchal. Regimes of droplet train impact on a moving surface in an additive manufacturing process. *Journal of Materials Processing Technology*, 210:550–559, 2010. ISSN 09240136. doi: 10.1016/j.jmatprotec.2009.10.018.

[19] T Foister. The Kinetics of Displacement Wetting in Liquid / Liquid / Solid Systems [II. *Interface*, 136(1), 1990.

[20] David Fuchs. The format of TEX's DVI files version 1. *TUGboat*, 2(2):12–16, July 1981.

[21] David Fuchs. Device independent file format. *TUGboat*, 3(2):14–19, October 1982.

[22] J Fukai, Y Shiiba, T Yamamoto, O Miyatake, D Poulikakos, C M Megaridis, and Z Zhao. Wetting effects on the spreading of a liquid droplet surface : Experiment and modeling colliding with a flat. *Physics of Fluids*, 7(2):236–247, 1995. ISSN 10706631. doi: 10.1063/1.868622. URL http://link.aip.org/link/?PHFLE6/7/236/1.

[23] Richard K. Furuta and Pierre A. MacKay. Two TEX implementations for the IBM PC. *Dr. Dobb's Journal*, 10(9):80–91, September 1985.

[24] P H Gregory, E J Guthrie, and M E Bunce. Experiments on splash dispersal of fungus spores. *Journal of general microbiology*, 20(2):328–354, 1959. ISSN 0022-1287. doi: 10.1099/00221287-20-2-328.

[25] Daryl Grunau, Shiyi Chen, and Kenneth Eggert. A lattice Boltzmann model for multiphase fluid flows. *Physics of Fluids A: Fluid Dynamics*, 5(10):2557, 1993. ISSN 08998213. doi: 10.1063/1.858769. URL http://arxiv.org/abs/comp-gas/9303001%5Cnhttp://scitation.aip.org/content/aip/

[26] Andrew K. Gunstensen, Daniel H. Rothman, Stéphane Zaleski, and Gianluigi Zanetti. Lattice Boltzmann model of immiscible fluids. *Physical Review A*, 43 (8):4320–4327, 1991. ISSN 10502947. doi: 10.1103/PhysRevA.43.4320.

[27] H. Heidarifatasmi and Ö. Ertunç. Simulations of Droplet Impacts on Hydrophobic Moving Walls. *ICCFD9 Proceedings*, 2016.

[28] C W HIRT and B D NICHOLS. Volume of fluid/VOF/ method for the dynamics of free boundaries. *Journal of Computational Physics*, 39(1):201–225, 1981. ISSN 00219991. doi: 10.1016/0021-9991(81)90145-5.

[29] C. W. Hirt, B. D. Nichols, and N. C. Romero. SOLA: A numerical solution algorithm for transient fluid flows. *NASA STI/Recon Technical Report N*, 75, January 1975.

[30] P V Hobbs and T Osheroff. Splashing of drops on shallow liquids. *Science (New York, N.Y.)*, 158(3805):1184–1186, 1967. ISSN 0036-8075. doi: 10.1126/science.158.3805.1184.

[31] L. M. Hocking and A D Rivers. The spreading of a drop by capillary action. *Journal of Fluid Mechanics*, 121(-1):425, 1982. ISSN 0022-1120. doi: 10.1017/S0022112082001979.

[32] R Hoffman, Monsanto Polymers, Petrochemicals Company, and Indian Orchard. A Study of the Advancing Interface I . Interface Shape in Liquid-Gas Systems. *Journal of Colloid and Interface Science*, 50(2):228–241, 1975. ISSN 00219797. doi: 10.1016/0021-9797(75)90225-8.

[33] SF. Kistler. Hydrodynamics of wetting. In: Berg JC, editor. Wettability. New York: Marcel Dekker. *Journal of Dispersion Science and Technology*, 14(6):

717–718, 1993. ISSN 0193-2691. doi: 10.1080/01932699308943443. URL http://www.tandfonline.com/doi/abs/10.1080/01932699308943443.

[34] Donald E. Knuth. The WEB system for structured documentation, version 2.3. Technical Report STAN-CS-83-980, Computer Science Department, Stanford University, Stanford, California, September 1983.

[35] Donald E. Knuth. Literate programming. *The Computer Journal*, 27(2):97–111, May 1984.

[36] Donald E. Knuth. *The TEX Book*. Addison-Wesley, Reading, Massachusetts, 1984. Reprinted as Vol. A of *Computers & Typesetting*, 1986.

[37] Donald E. Knuth. A torture test for TEX, version 1.3. Technical Report STAN-CS-84-1027, Computer Science Department, Stanford University, Stanford, California, November 1984.

[38] Donald E. Knuth. *TEX: The Program*, volume B of *Computers & Typesetting*. Addison-Wesley, Reading, Massachusetts, 1986.

[39] Leslie Lamport. *LATEX: A Document Preparation System. User's Guide and Reference Manual*. Addison-Wesley, Reading, Massachusetts, 1986.

[40] M B Lesser and J E Field. The Impact of Compressible Liquids. *Annual Review of Fluid Mechanics*, 15(1):97–122, 1983. ISSN 0066-4189. doi: 10.1146/annurev.fl.15.010183.000525.

[41] H. Liu, S. Krishnan, S. Marella, and H.S. Udaykumar. Sharp interface Cartesian grid method II: A technique for simulating droplet interactions with surfaces of arbitrary shape. *Journal of Computational Physics*, 210(1): 32–54, nov 2005. ISSN 00219991. doi: 10.1016/j.jcp.2005.03.032. URL http://linkinghub.elsevier.com/retrieve/pii/S0021999105001968.

[42] Siddhartha F. Lunkad, Vivek V. Buwa, and K. D P Nigam. Numerical simulations of drop impact and spreading on horizontal and inclined surfaces. *Chemical Engineering Science*, 62(24):7214–7224, 2007. ISSN 00092509. doi: 10.1016/j.ces.2007.07.036.

[43] Abraham Marmur. Wetting on hydrophobic rough surfaces: To be heterogeneous or not to be? *Langmuir*, 19(20):8343–8348, 2003. ISSN 07437463. doi: 10.1021/la0344682.

[44] V. Mehdi-Nejad, J. Mostaghimi, and S. Chandra. Air bubble entrapment under an impacting droplet. *Physics of Fluids*, 15(1):173–183, 2003. ISSN 10706631. doi: 10.1063/1.1527044.

[45] a. J B Milne and a. Amirfazli. The Cassie equation: How it is meant to be used. *Advances in Colloid and Interface Science*, 170(1-2):48–55, 2012. ISSN 00018686. doi: 10.1016/j.cis.2011.12.001. URL http://dx.doi.org/10.1016/j.cis.2011.12.001.

[46] Cheng Ming and Lou Jing. Lattice Boltzmann simulation of a drop impact on a moving wall with a liquid film. *Computers and Mathematics with Applications*, 67(2):307–317, 2014. ISSN 08981221. doi: 10.1016/j.camwa.2013.07.003. URL http://dx.doi.org/10.1016/j.camwa.2013.07.003.

[47] Chr. Mundo, M Sommerfeld, and C Tropea. Droplet-wall collisions: Experimental studies of the deformation and breakup process. *Int. J. Multiph. Flow*, 21(2):151–173, 1995. ISSN 03019322. URL http://www.scopus.com/inward/record.url?eid=2-s2.0-0029278456&partnerID=40&md5

[48] Metin Muradoglu and Savas Tasoglu. A front-tracking method for computational modeling of impact and spreading of viscous droplets on solid walls. *Computers & Fluids*, 39(4):615–625, apr 2010. ISSN 00457930. doi: 10.1016/j.compfluid.2009.10.009. URL http://linkinghub.elsevier.com/retrieve/pii/S0045793009001698.

[49] R.R. Nourgaliev, T.N. Dinh, T.G. Theofanous, and D. Joseph. The lattice Boltzmann equation method: theoretical interpretation, numerics and implications. *International Journal of Multiphase Flow*, 29(1):117–169, 2003. ISSN 03019322. doi: 10.1016/S0301-9322(02)00108-8.

[50] S OSHER and J A SETHIAN. Fronts Propagating With Curvature-Dependent Speed - Algorithms Based on Hamilton-Jacobi Formulations. *Journal of Computational Physics*, 79(1):12–49, 1988. ISSN 0021-9991. doi: 10.1016/0021-9991(88)90002-2.

[51] M. Pasandideh-Fard, Y. M. Qiao, S. Chandra, and J. Mostaghimi. Capillary effects during droplet impact on a solid surface. *Physics of Fluids*, 8(3):650, 1996. ISSN 10706631. doi: 10.1063/1.868850. URL http://link.aip.org/link/?PHFLE6/8/650/1.

[52] M. Pasandideh-Fard, S. Chandra, and J. Mostaghimi. A three-dimensional model of droplet impact and solidification. *International Journal of Heat and Mass Transfer*, 45(11):2229–2242, 2002. ISSN 00179310. doi: 10.1016/S0017-9310(01)00336-2.

[53] Oren Patashnik. *Designing BibTEX Styles*. Computer Science Department, Stanford University, January 1988.

[54] Oren Patashnik. *BibTEXing*. Computer Science Department, Stanford University, Stanford, California, January 1988. Available in the BibTEX release.

[55] a Prosperetti. The Impact of Drops on Liquid Surfaces and the Underwater Noise of Rain. *Annual Review of Fluid Mechanics*, 25(1):577–602, 1993. ISSN 00664189. doi: 10.1146/annurev.fluid.25.1.577.

[56] Martin Rein. Phenomena of liquid drop impact on solid and liquid surfaces. *Fluid Dynamics Research*, 12(2):61–93, 2009. ISSN 0169-5983. doi: 10.1016/0169-5983(93)90106-K.

[57] Michael Renardy, Yuriko Renardy, and Jie Li. Numerical Simulation of Moving Contact Line Problems Using a Volume-of-Fluid Method. *Journal of Computational Physics*, 171(1):243–263, 2001. ISSN 00219991. doi: 10.1006/jcph.2001.6785. URL http://www.scopus.com/inward/record.url?eid=2-s2.0-0001532298&partnerID=tZOtx3

[58] S. N. Reznik and A. L. Yarin. Spreading of a viscous drop due to gravity and capillarity on a horizontal or an inclined dry wall. *Physics of Fluids*, 14(1): 118–132, 2002. ISSN 10706631. doi: 10.1063/1.1426388.

[59] R Rioboo, Cam Tropea, and M Marengo. Outcomes from a drop impact on solid surfaces. *At. Sprays*, 11(2):155–165, 2001. ISSN 10445110. URL http://www.scopus.com/inward/record.url?eid=2-s2.0-0035295137&partnerID=tZOtx3

[60] R. Rioboo, M. Marengo, and C. Tropea. Time evolution of liquid drop impact onto solid, dry surfaces. *Experiments in Fluids*, 33(1):112–124, jul 2002. ISSN 0723-4864. doi: 10.1007/s00348-002-0431-x. URL http://link.springer.com/10.1007/s00348-002-0431-x.

[61] R Rioboo, C Bauthier, J Conti, M Vou, and J De Coninck. Experimental investigation of splash and crown formation during single drop impact on wetted surfaces, 2003. ISSN 0723-4864.

[62] I.V. Roisman, L. Opfer, C. Tropea, M. Raessi, J. Mostaghimi, and S. Chandra. Drop impact onto a dry surface: Role of the dynamic contact angle. *Colloids and Surfaces A: Physicochemical and Engineering Aspects*, 322(1-3): 183–191, 2008. ISSN 09277757. doi: 10.1016/j.colsurfa.2008.03.005. URL http://linkinghub.elsevier.com/retrieve/pii/S0927775708001738.

[63] F. J. Montes Ruiz-Cabello, M. A. Rodrguez-Valverde, and M. A. Cabrerizo-Vilchez. Contact angle hysteresis on polymer surfaces: An experimental study. *Journal of Adhesion Science and Technology*, 25(16):2039–2049, 2011. doi: 10.1163/016942410X544848. URL http://dx.doi.org/10.1163/016942410X544848.

[64] Arthur L. Samuel. First grade TEX: A beginner's TEX manual. Technical Report SATN-CS-83-985, Computer Science Department, Stanford University, Stanford, California, November 1983.

[65] Ruben Scardovelli and Stéphane Zaleski. Direct Numerical Simulation of Free-Surface and Interfacial Flow. *Annual Review of Fluid Mechanics*, 31(1):567–603, 1999. ISSN 0066-4189. doi: 10.1146/annurev.fluid.31.1.567.

[66] J. A. Sethian. *Level Set Methods and Fast Marching Methods*. Cambridge University Press, second edition edition, 1999.

[67] Yulii D Shikhmurzaev. Spreading of drops on solid surfaces in a quasi-static regime. *Physics of Fluids*, 9(1997):

266, 1997. ISSN 10706631. doi: 10.1063/1.869147. URL http://scitation.aip.org/content/aip/journal/pof2/9/2/10.1063/1.869147.

[68] S Sikalo, C Tropea, and E N Ganić. Impact of droplets onto inclined surfaces. *Journal of colloid and interface science*, 286(2):661–9, jun 2005. ISSN 0021-9797. doi: 10.1016/j.jcis.2005.01.050. URL http://www.ncbi.nlm.nih.gov/pubmed/15897085.

[69] Š Šikalo, H. D. Wilhelm, I. V. Roisman, S. Jakirlić, and C. Tropea. Dynamic contact angle of spreading droplets: Experiments and simulations. *Physics of Fluids*, 17(6):1–13, 2005. ISSN 10706631. doi: 10.1063/1.1928828.

[70] Michael D. Spivak. *The Joy of TEX*. American Mathematical Society, 1985.

[71] C. D. Stow and M. G. Hadfield. An Experimental Investigation of Fluid Flow Resulting from the Impact of a Water Drop with an Unyielding Dry Surface. *Proceedings of the Royal Society A: Mathematical, Physical and Engineering Sciences*, 373(1755):419–441, 1981. ISSN 1364-5021. doi: 10.1098/rspa.1981.0002.

[72] R D Stow, C.D., Stainer. The Physical Products of a Splashing Water Drop. *J. Meteorol. Soc. Japan*, 55(5):518–532, 1977.

[73] Mark Sussman, Peter Smereka, and Stanley Osher. A Level Set Approach for Computing Solutions to Incompressible Two-Phase Flow, 1994. ISSN 00219991. URL http://www.sciencedirect.com/science/article/pii/S0021999184711557.

[74] Rafael Tadmor. Line energy and the relation between advancing, receding, and Young contact angles. *Langmuir*, 20(18):7659–7664, 2004. ISSN 07437463. doi: 10.1021/la049410h.

[75] Konrad Terpilowski, Lucyna Holysz, and Emil Chibowski. Surface free energy of sulfur-Revisited. II. Samples solidified against different solid surfaces. *Journal of Colloid and Interface Science*, 319(2):514–519, 2008. ISSN 00219797. doi: 10.1016/j.jcis.2007.10.054.

[76] S. T. Thoroddsen, T. G. Etoh, K. Takehara, N. Ootsuka, and Y. Hatsuki. The air bubble entrapped under a drop impacting on a solid surface. *Journal of Fluid Mechanics*, 545:203, 2005. ISSN 0022-1120. doi: 10.1017/S0022112005006919.

[77] Tuan Tran, Hélène de Maleprade, Chao Sun, and Detlef Lohse. Air entrainment during impact of droplets on liquid surfaces. *Journal of Fluid Mechanics*, 726:R3, 2013. ISSN 0022-1120. doi: 10.1017/jfm.2013.261. URL http://www.journals.cambridge.org/abstract_S0022112013002619.

[78] G Tryggvason, B Bunner, A Esmaeeli, D Juric, N Al-Rawahi, W Tauber, J Han, S Nas, and Y J Jan. A front-tracking method for the computations of multiphase flow. *Journal of Computational Physics*, 169(2):708–759, 2001. ISSN 00219991. doi: DOI 10.1006/jcph.2001.6726.

[79] Salih Ozen Unverdi and Gr??tar Tryggvason. A front-tracking method for viscous, incompressible, multi-fluid flows. *Journal of Computational Physics*, 100 (1):25–37, 1992. ISSN 10902716. doi: 10.1016/0021-9991(92)90307-K.

[80] M. Van Dyke. *Perturbation Methods in Fluid Mechanics*. Parabolic Press, 1975. ISBN 9780915760015. URL https://books.google.com.tr/books?id=jwBRAAAAMAAJ.

[81] a. B. Wang and C. C. Chen. Splashing impact of a single drop onto very thin liquid films. *Physics of Fluids*, 12(9):2155–2158, 2000. ISSN 10706631. doi: 10.1063/1.1287511.

[82] Robert N Wenzel. Resistance of solid surfaces to wetting by water. *Journal of Industrial and Engineering Chemistry (Washington, D. C.)*, 28:988–994, 1936. ISSN 0095-9014. doi: 10.1021/ie50320a024.

[83] Gene Whyman, Edward Bormashenko, and Tamir Stein. The rigorous derivation of Young, Cassie-Baxter and Wenzel equations and the analysis of the contact angle hysteresis phenomenon. *Chemical Physics Letters*, 450(4-6):355–359, 2008. ISSN 00092614. doi: 10.1016/j.cplett.2007.11.033.

[84] Gershon Wolansky and Abraham Marmur. Apparent contact angles on rough surfaces: The Wenzel equation revisited. *Colloids and Surfaces A: Physicochemical and Engineering Aspects*, 156(1-3):381–388, 1999. ISSN 09277757. doi: 10.1016/S0927-7757(99)00098-9.

[85] Arthur Mason Worthington. *A Study of Splashes*. Longmans, Green, and Company, 1908, 1908. URL https://books.google.com.tr/books/about/A_Study_of_Splashes.html?id=LtdUAAAAQAA

[86] A L Yarin and D A Weiss. Impact of drops on solid surfaces: self-similar capillary waves, and splashing as a new type of kinematic discontinuity, 1995. ISSN 0022-1120.

[87] A.L. Yarin. DROP IMPACT DYNAMICS: Splashing, Spreading, Receding, Bouncing.... *Annual Review of Fluid Mechanics*, 38(1):159–192, 2006. ISSN 0066-4189. doi: 10.1146/annurev.fluid.38.050304.092144.

[88] Tain Shi Zen, Fu Chu Chou, and Ju Lung Ma. Ethanol drop impact on an inclined moving surface. *Int. Commun. Heat Mass Transf.*, 37(8):1025–1030, 2010.

VITA

vita needs to be copied here.